

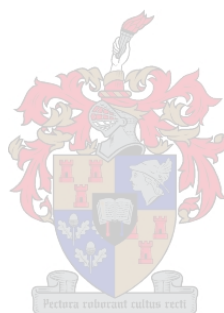
Self-assembly of new porous materials

by

Tia Jacobs

Submitted in partial fulfilment of the requirements for the degree

Doctor of Philosophy



at

Stellenbosch University

Department of Chemistry and Polymer Science

Faculty of Science

Supervisor: Prof. L. J. Barbour

Co-Supervisor: Dr. M. W. Bredenkamp

Date: March 2009

molecule in one void does not influence the orientation of the guest in the neighbouring void along [001]. Therefore the guest molecules are most likely statistically (*i.e.* 50/50) disordered throughout the structure such that no localised polar ordering exists.

It is clear from the guest space-filling diagram (Figure 3.8b) that the three chlorine atoms arranged around the three-fold axis are in close contact with the host, since they protrude visibly from the surface that maps the van der Waals cavity (grey surface). The roof and ceiling of the cavity are bounded by six-membered $\cdots\text{O}-\text{H}\cdots\text{O}\cdots$ hydrogen bonded rings where the $\text{O}\cdots\text{O}$ distance is 2.7995(12) Å.

The structure of 2_{CCl_4} is analogous to that of 1_{CCl_4} , with lattice parameters $a = b = 26.632(2)$ and $c = 12.0349(17)$ Å, with the exception that two molecules of carbon tetrachloride now reside within each cavity. Both of these guest molecules are disordered over two positions (Figure 3.9) of equal occupancy (*i.e.* each with a site-occupancy factor that is required by space group symmetry to be 0.5). In this structure the hourglass-shaped cavity is stabilised by the $\cdots\text{S}-\text{H}\cdots\text{S}\cdots$ hydrogen bonded ring where $\text{S}\cdots\text{S}$ distance is 3.7858(8) Å. This is just greater than the sum of the $\text{S}\cdots\text{S}$ van der Waals radii (3.60 Å) and, as shown below, constitutes a weak interaction. Figure 3.9a shows the two self-consistent possibilities for CCl_4 occupation of the voids in yellow and green. The two disorder-related locations of the pair of carbon tetrachloride molecules in each cavity are related to one another by $\bar{3}$ site symmetry.

It is interesting to rationalise the possibilities for polar alignment of the guest molecules in the crystal. If one considers the crystal to be defect-free, then all of the guest molecules within a single column must be aligned in the same direction (*i.e.* in a crystallographically polar fashion) as a result of spatial constraints. Figure 3.9b shows both orientations of the guest molecules as they are aligned along a vector defined by the $\text{C}\rightarrow\text{Cl}$ bond that is parallel to the three-fold axis. If guests are aligned in a single column as suggested (either the green or the yellow orientation, Figure 3.9), guest arrangement in the neighbouring channels can be aligned in either a parallel or anti-parallel orientation (with a 50/50 probability of alignment in either direction), resulting in an overall non-polar arrangement of guests in the crystal.

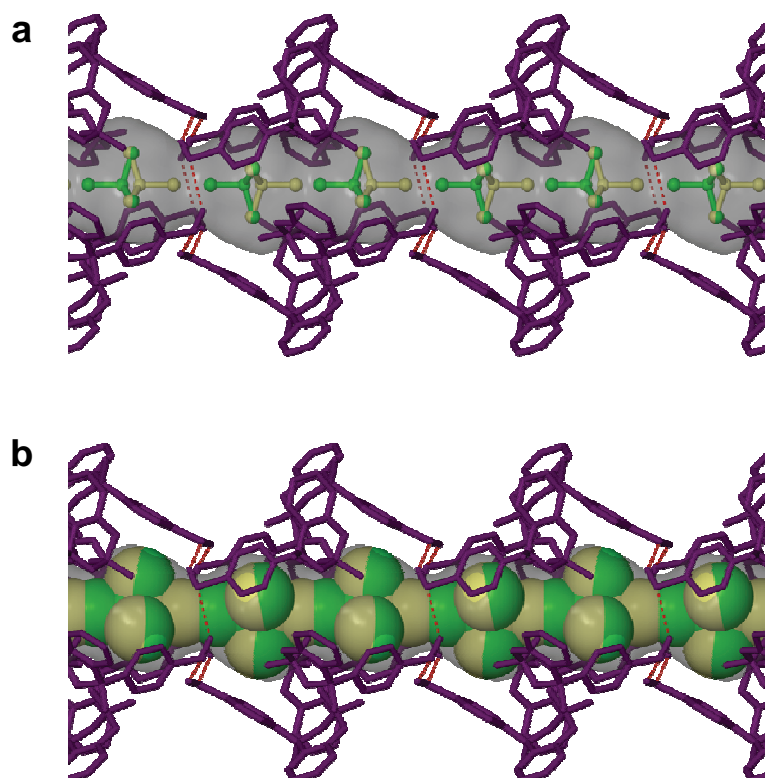


Figure 3.9 Supramolecular assembly of 2_{CCl_4} viewed perpendicular to [001]. The racemic host molecules are shown in purple and the two 50% disordered positions of the guest carbon tetrachloride molecules are indicated in green and yellow. **(a)** Ball-and-stick and **(b)** van der Waals space-filling models. Six molecules of **2** are joined together by hydrogen bonding (shown as dashed red lines) and stacking of these hexameric units along [001] produces guest-accessible voids (grey surface). All hydrogen atoms, except those of the thiol-moieties have been omitted for clarity.

Structure 3_{CCl_4} crystallises in the chiral space group $R3$ (note the reduction in symmetry from the centrosymmetric space group $R\bar{3}$ obtained for 1_{CCl_4} and 2_{CCl_4}) with lattice parameters $a = b = 26.6670(16)$ and $c = 11.7710(14)$ Å. The expected quasi-racemic structure is obtained, with two molecules of carbon tetrachloride included in each cavity. The roof and ceiling of each cavity are defined by hexameric $\cdots\text{O}-\text{H}\cdots\text{S}-\text{H}\cdots$ hydrogen bonded rings where $\text{O}_{\text{donor}}\cdots\text{S}_{\text{acceptor}} = 3.427(3)$ and $\text{S}_{\text{donor}}\cdots\text{O}_{\text{acceptor}} = 3.527(3)$ Å. As illustrated in Figure 3.10a, the guest molecules can once again adopt two opposite orientations as observed in 2_{CCl_4} (shown in yellow and green). However, in this case the two positions are not related to one another by crystallographic symmetry (*i.e.* owing to the absence of inversion symmetry) and there is a noticeable head-to-tail guest ordering in the column along [001] (previously unobserved for 1_{CCl_4} and 2_{CCl_4}). We propose that the guest ordering is due to a combination of electrostatic preference and spatial constraints. The site occupancy

factors of the yellow and green instances were allowed to refine with the only constraint being that the sum of their occupancies must be unity (in the case of 1_{CCl_4} and 2_{CCl_4} a 50/50 directional disorder was dictated by crystallographic symmetry). According to the refinement against intensity data, the carbon tetrachloride guest orientation designated in green in Figure 3.10b (*i.e.* with its crystallographic three-fold C→Cl bond aligned along the mean vector of the C→OH bonds) occurs with a probability of 88%.[†] This distinguishes the inclusion system of 3_{CCl_4} from those of 1_{CCl_4} and 2_{CCl_4} in that guests in neighbouring columns of **3** are now arranged in a parallel fashion with an 88% probability of pointing in one direction and a 12% probability of pointing in the opposite direction – *i.e.* that the arrangement is polar overall. Bulk polar alignment is thus achieved and, interestingly, there exists no obvious method of communication between adjacent channels.¹⁷ Even without

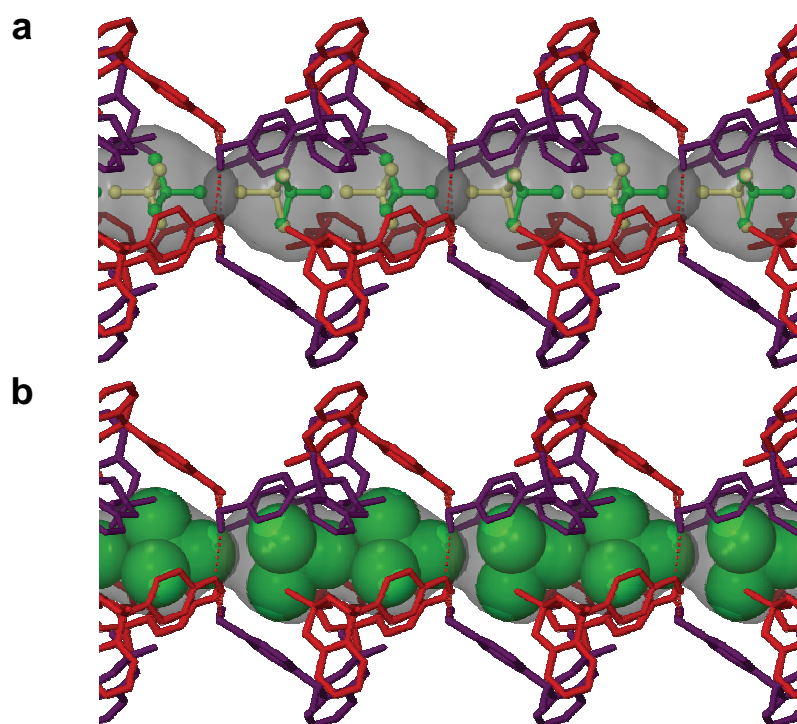


Figure 3.10 Supramolecular assembly of 3_{CCl_4} shown perpendicular to [001]. The (*R*)-**1** and the (*S*)-**2** molecules are shown in red and purple, respectively. (a) The disorder of the guest carbon tetrachloride molecules are represented as green and yellow ball-and-stick figures and (b) the preferred carbon tetrachloride orientation shown in van der Waals space-filling representation so that the C→Cl bond aligns with the mean vector of the O→H bonds. The cavities formed by the host due to interdigitation of enantiomers of **1** and **2** along [001] are shown as a grey surface. All hydrogen atoms, except those of the hydroxy- and thiol-moieties have been omitted for clarity.

[†] With multiple least squares refinement cycles of 3_{CCl_4} the free variable associated with the site occupancy factors of the guest molecules does not vary significantly from 0.8794(19).

considering the guest molecules, it is conceivable that neighbouring columns would not have to assume a polar structure (only one that is chiral). However, the host molecules choose to assemble in a polar fashion, and this arrangement is therefore transferred to the guest molecules.

Figure 3.11 illustrates the relative 'pore' sizes (*i.e.* the size of the hydrogen bonded ring defining the floor and ceiling of each cavity) of 1_{CCl_4} – 3_{CCl_4} and shows that an intermediate 'pore' size has effectively been engineered in the case of 3_{CCl_4} .

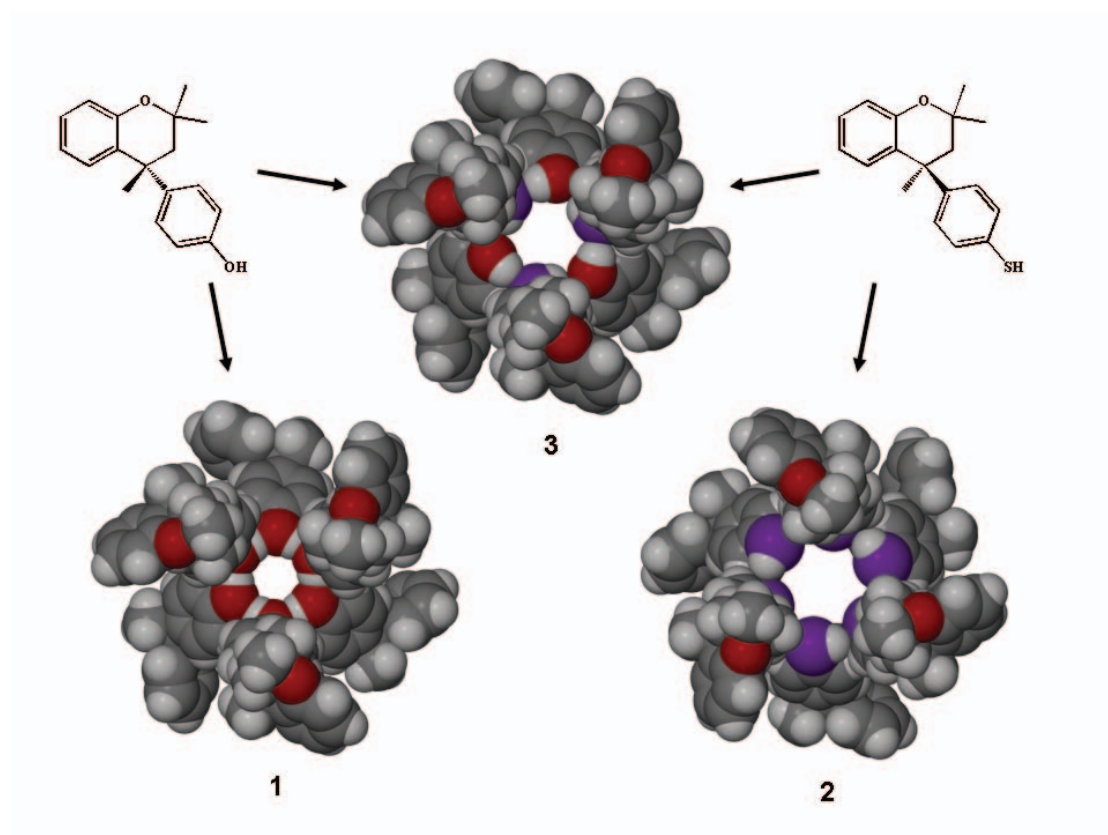


Figure 3.11 Projections illustrating the different size of the hydrogen bonded ring apertures (viewed along [001]) for the 4-*p*-hydroxyphenyl-2,2,4-trimethylchroman **1**, 4-*p*-mercaptophenyl-2,2,4-trimethylchroman **2** and quasi-racemic clathrate **3**.

3.2.3 Desorption of 1_{CCl_4} , 2_{CCl_4} and 3_{CCl_4} : thermal analysis, X-ray powder diffraction and scanning electron microscopy

The carbon tetrachloride clathrates of **1-3** were studied by thermogravimetry (TGA) to confirm the host:guest ratios and to determine the temperature range of guest desorption. Differential scanning calorimetry (DSC) was carried out to establish

onset temperatures for guest-release and to determine whether concomitant phase transitions occur upon guest desorption. Thermograms were recorded using a heating rate of $2.5\text{ }^{\circ}\text{C}\cdot\text{min}^{-1}$ and guest losses were observed at onset temperatures (T_{on}) of 154.2, 74.1 and 66.8 $^{\circ}\text{C}$ for compounds **1-3**, respectively, corresponding to host:guest ratios of 3:1 and 3.53:1 for compounds **2** and **3** (Figure 3.12).[‡] The higher than expected host:guest ratio for compound **3** was attributed to the presence of enantiomerically pure crystals (of (*R*)-**1** and (*S*)-**2**), which contain no solvent and would thus lower the overall guest:host ratio. Analysis of the single-crystal structure of $\mathbf{3}_{\text{CCl}_4}$ using SQUEEZE indicated the number of electrons within each guest-accessible cavity to be 148.8. This result is in good agreement with the presumed presence of two molecules of carbon tetrachloride per cavity (*i.e.* 74 electrons per molecule). In the case of compound **1**, it was also not possible to accurately determine the host:guest ratio from thermogravimetry because desolvation and sublimation of the host both occur within a narrow temperature range. The first step in the curve (Figure 3.12a) corresponds to a 16.1% weight loss, which is approximately equivalent to two molecules of carbon tetrachloride per cavity.

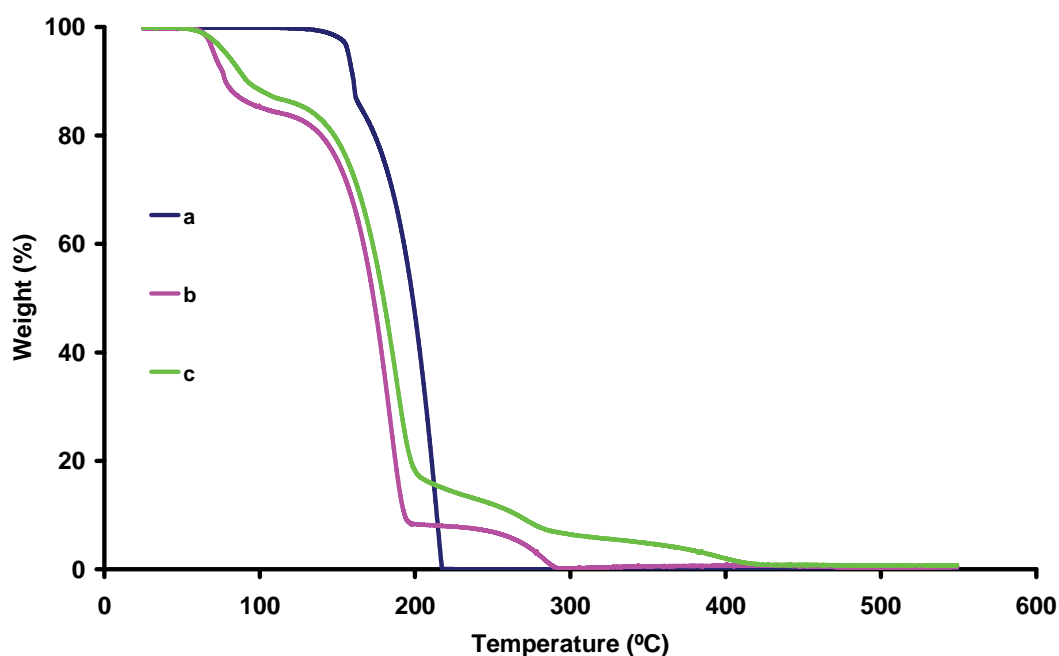


Figure 3.12 TGA traces showing onset temperatures of (a) 154.2 $^{\circ}\text{C}$ for $\mathbf{1}_{\text{CCl}_4}$, (b) 74.1 $^{\circ}\text{C}$ for $\mathbf{2}_{\text{CCl}_4}$ and (c) 66.8 $^{\circ}\text{C}$ for $\mathbf{3}_{\text{CCl}_4}$.

[‡] According to the TGA traces (Figure 3.12), weight loss occurs as multi-step processes in all three cases and the minimum in the first derivative of the weight-loss curve was used to determine the end of the first desolvation step.

However, using single-crystal diffraction data and SQUEEZE (74.4 electrons/cavity), it appears that there is only one guest molecule per cavity.

Initial DSC analysis of $\mathbf{1}_{\text{CCl}_4}$ revealed a single endotherm at *ca* 157 °C. To determine whether this represents a true melt, the sample was heated at different rates and the onset temperatures of the resulting endotherms were compared. Figure 3.13 shows that the onset temperatures occur consistently at 158 °C for the four chosen ramp rates of 2.5, 5, 10 and 20 °C.min⁻¹. A sample of sublimed $\mathbf{1}$ (*i.e.* guest-free, but with the same host structure as $\mathbf{1}_{\text{CCl}_4}$) was also analysed. In this case a slightly lower (by 1 °C) value of T_{on} was recorded. Although the difference in T_{on} is not considerable, this subtle difference can be attributed to the slight increase in the stability of the structure afforded by the presence of the CCl₄ guest. The same phenomenon was observed when the toluene clathrate was subjected to a similar experiment, except that the toluene clathrate appears to be even more stable.

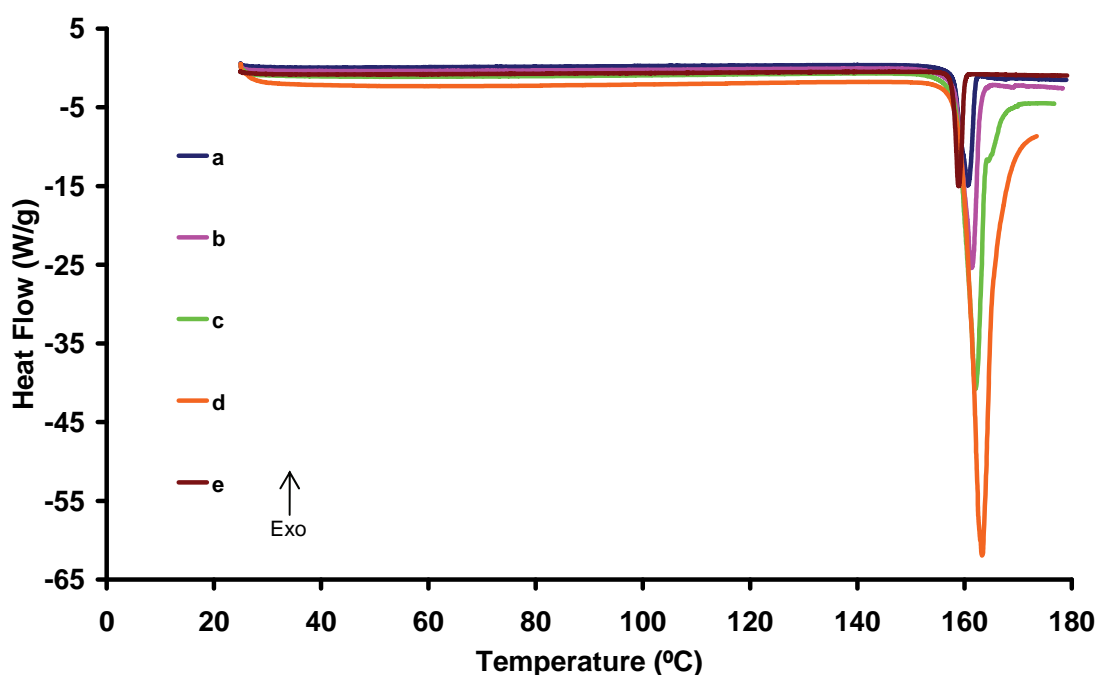


Figure 3.13 DSC curves for $\mathbf{1}_{\text{CCl}_4}$ with different heating rates (a) 2.5 °C.min⁻¹, (b) 5 °C.min⁻¹, (c) 10 °C.min⁻¹, (d) 20 °C.min⁻¹ and (e) sublimed guest-free $\mathbf{1}$ at 2.5 °C.min⁻¹.

Figure 3.14a shows the DSC trace recorded for $\mathbf{2}_{\text{CCl}_4}$ in which an initial endotherm with a peak maximum of 78 °C represents a phase change upon guest loss, followed by a larger endotherm with an onset temperature of 105.8 °C. Endotherms in this latter region are also evident for a sample of $\mathbf{2}_{\text{CCl}_4}$ that had been heated at 65 °C for 12

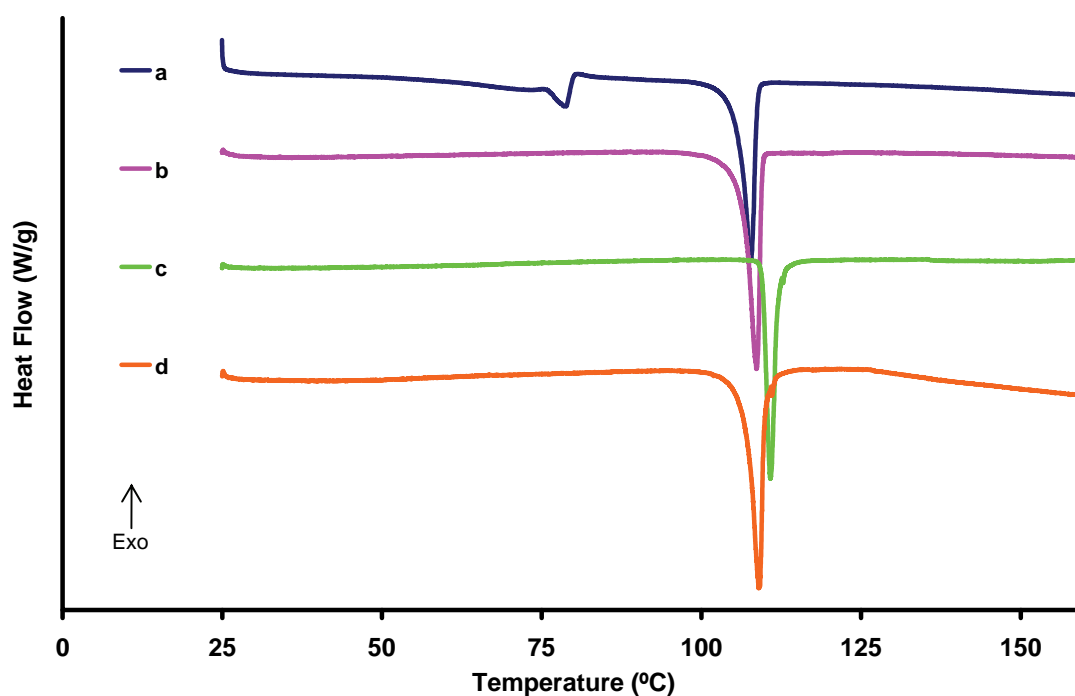


Figure 3.14 DSC curves for (a) the carbon tetrachloride clathrate 2_{CCl_4} , (b) 2_{CCl_4} after guest desorption, (c) sublimed **2** and (d) **2** crystallised from cyclohexane.

hours, a sublimed sample of **2** (at 90 °C and 0.1 mbar) and **2** crystallised from cyclohexane (Figure 3.14b-d), with onset temperatures of 106.3, 104.6 and 109.5 °C, respectively.

XRPD analysis shows that, upon guest desorption of 2_{CCl_4} , the host molecules resolve into their enantiomerically pure phases (structure described in 3.1), albeit as a mixture of (*R*)-**2** and (*S*)-**2** powder phases. This resolved phase can also be obtained when a sample of **2** is sublimed, or if **2** is crystallised from cyclohexane. Figure 3.15 shows the XRPD patterns of bulk samples of 2_{CCl_4} before and after desorption. These patterns match those simulated from the single-crystal structures of 2_{CCl_4} and resolved **2**, respectively. The possible reversibility of the desorption process was investigated by exposing desorbed **2** to carbon tetrachloride vapour. After 60 hours no weight gain was observed, from which it is concluded that the guest-desorption process is irreversible. Clearly the racemic (and therefore potentially porous) host phase is destroyed upon desolvation of the CCl_4 clathrate. It was supposed that this may, at least in part, be due to the large size of the guest relative to the size of the $\cdots\text{S}-\text{H}\cdots$ hydrogen bonded aperture. To investigate whether removal of a smaller guest might leave the host framework intact, **2** was crystallised from acetonitrile (MeCN).

Acetonitrile was selected for its ability as a solvent for **2** and also because of its linear shape. Slow evaporation of a concentrated solution of **2** in MeCN afforded only a white powder which was identified by XRPD analysis as the chiral phase rather than that of the hoped-for clathrate.

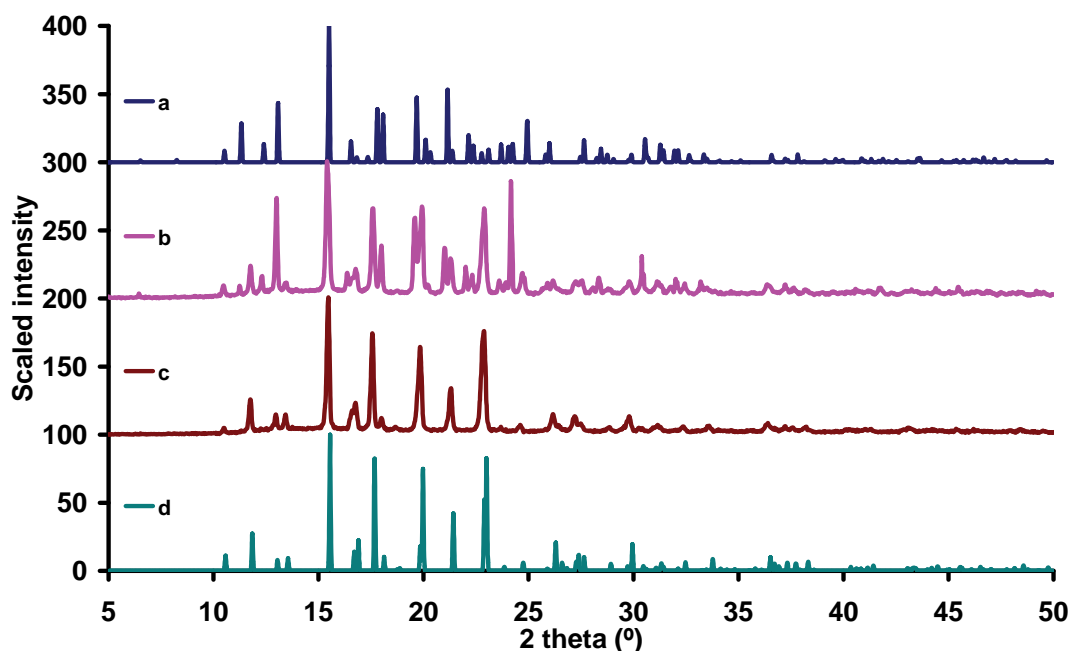


Figure 3.15 (a) XRPD pattern simulated from the single-crystal structure of 2_{CCl_4} and experimentally determined XRPD patterns for 2_{CCl_4} (b) before desorption, (c) after desorption and (d) powder pattern calculated from the single-crystal structure of sublimed **2**.

Similar observations were made using 3_{CCl_4} . Figure 3.16 shows an excellent match between the powder pattern of a bulk sample of 3_{CCl_4} and that simulated from the single-crystal clathrate structure. After the sample was heated at 70 °C for 24 hours the experimental pattern matches that calculated for resolved **1**, indicating that the clathrate resolves into the enantiomerically pure phases of **1** and **2** upon guest desorption. That peaks corresponding to resolved **2** are not as evident as those for resolved **1** and this is attributed to the greater crystallinity of resolved **1**.

In the hope of generating the β_0 -structure of **3** from MeCN (as attempted with **2**), equimolar amounts of (*R*)-**1** and (*S*)-**2** were crystallised from acetonitrile and the resulting powder was subjected to XRPD analysis. From Figure 3.17 it is evident that the clathrate structure does not form from acetonitrile since a powder pattern matching that of resolved **1** was obtained.

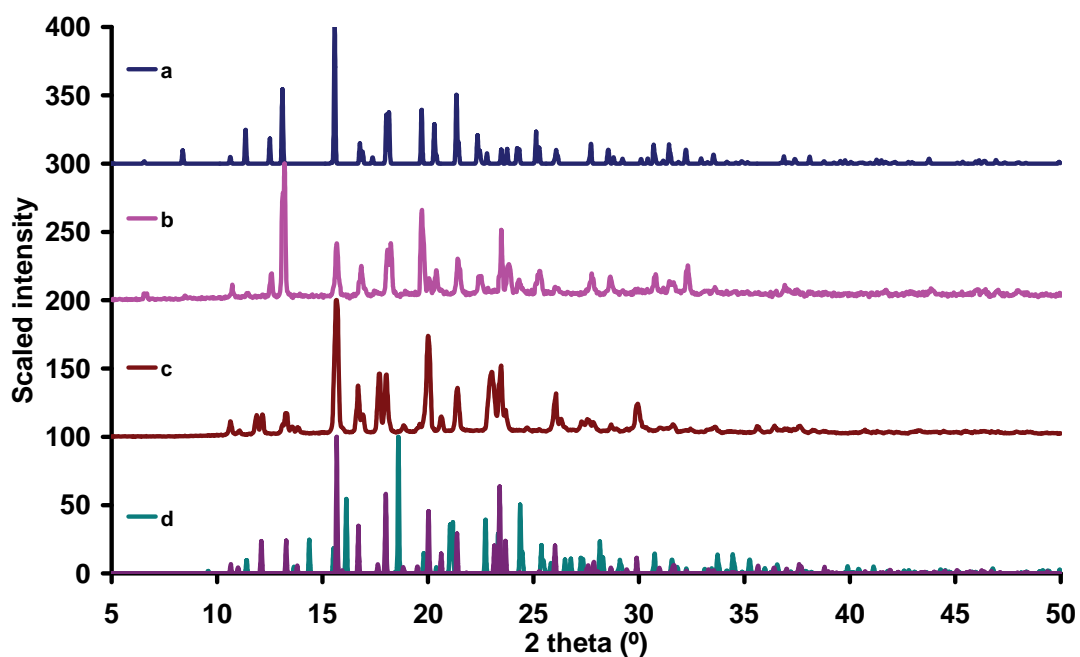


Figure 3.16 (a) XRPD diffractogram for 3_{CCl_4} simulated from single-crystal X-ray diffraction; and experimental powder patterns of 3_{CCl_4} (b) before and (c) after desorption. (d) Calculated powder traces for resolved 1 and resolved 2 shown in purple and green, respectively.

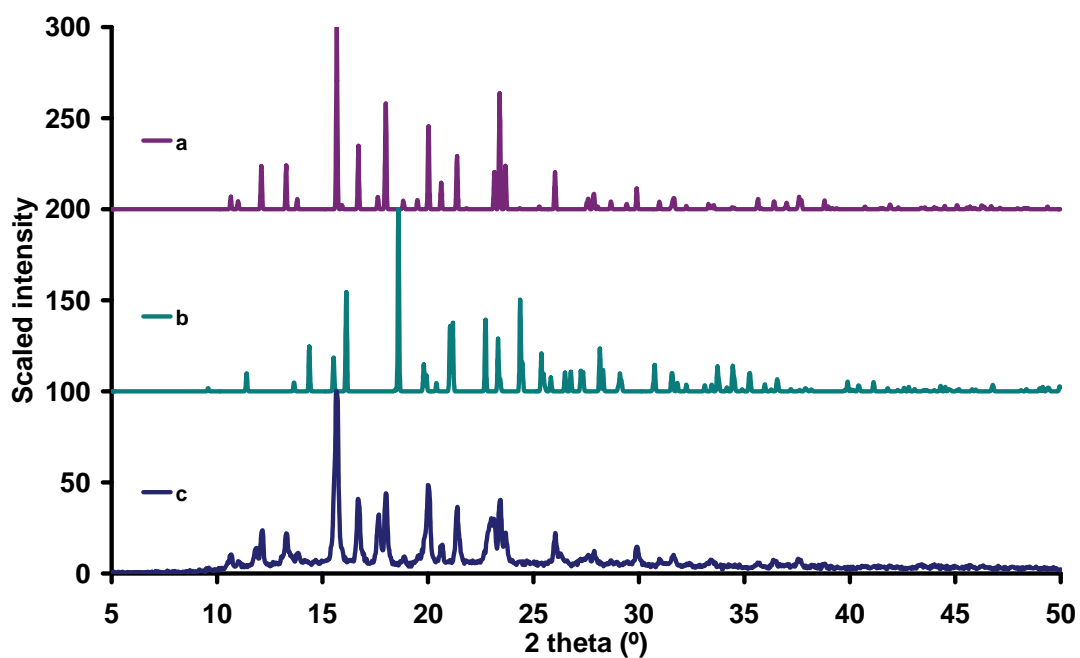


Figure 3.17 Calculated XRPD diffractograms of (a) resolved 1 and (b) resolved 2. (c) Experimental pattern of 3 deposited from MeCN.

The results described above emphasise the importance of the solvent templation-effect in the formation of the clathrates of compounds **2** and **3**. As previously mentioned, compound **1** can be grown in its β_0 -form by sublimation or crystallisation from a suitably large solvent. This can be attributed to two factors: (i) the significant host stabilisation gained from the hexameric hydrogen bonded ring and (ii) that the awkwardly-shaped DC molecules complement one another in the racemic clathrate form (*i.e.* van der Waals interactions). Evidently these factors provide enough of a stabilising influence to overcome the destabilisation due to the formation of a relatively large empty void. Compound **2** apparently only forms the clathrate in the presence of suitably sized guest molecules that complement the host shape, thus affording additional stability. This suggests that the stabilisation gained from the hexagonal $\cdots\text{S}-\text{H}\cdots\text{S}$ ring alone is not sufficient to maintain the racemic structure in its guest-free form, and that the stabilisation due to close-packing as well as the $\text{S}-\text{H}\cdots\text{O}$ hydrogen bonds and the edge-to-face π - π interactions between the chroman and the thiophenol moieties are more dominant. The same behaviour was observed in the case of **3** where the clathrate structure was formed using carbon tetrachloride as a template, but subsequent guest removal results in rearrangement into the enantiomerically pure phases. Since clathrates could not be formed from **2** or **3** in the presence of acetonitrile, we can conclude that it is important for guest molecules to be of the appropriate size, otherwise spontaneous resolution becomes energetically more favourable.

The concept behind the original objective of the study outlined in this chapter was successfully demonstrated (*i.e.* that the aperture size between neighbouring guest-accessible voids could be engineered using a rational design approach). However, it was disappointing to discover that the β_0 -phases of **2** and **3** are not energetically favourable. Nevertheless, the observations made as part of this study raise very interesting questions about the process of desolvation in general. Are the clathrates of **2**_{CCl₄} and **3**_{CCl₄} disassembling because of a mechanism tied to the conditions required for guest removal? A possible scenario is that, as guests escape from the clathrate material, a short-lived localised congregation of guest solvent molecules occurs on the surface of the particles. This may provide a set of physical conditions sufficient to solubilise the host at that location and to thus effect recrystallisation under critically solvent-poor circumstances. To clarify, this is not to be confused with melting as

there is no evidence from the DSC that either of the resolved forms **2** or **3** would melt at a temperature lower than 110 °C. Another scenario involves the commonly-held belief that simple rearrangement of host molecules occurs concomitantly with guest removal. This may involve a solid-state migration mechanism in which (*R*)- and (*S*)-enantiomers segregate within a crystal so that parts of the crystal are enriched with either (*R*)- or (*S*)-enantiomers (corresponding to the enantiomerically pure phase). Assuming the latter scenario (*i.e.* that desolvation is simply a process of rearrangement or solid state migration, rather than more dramatic recrystallisation) to hold true, one might expect that we would find both (*R*)- or (*S*)-enantiomers in a given particle, but that there would be regions that are enriched with either the (*R*) or (*S*). On the other hand, if desolvation involves a process of micro-recrystallisation, we might expect separation of the racemic mixture and recombination of the (*R*)- and (*S*)-enantiomers into *separate* particles (and these may possibly even be slightly larger particles – or crystals – than those afforded by the rearrangement process). In solvates of molecular crystals (generally of organic inclusion compounds) it is well-established that host rearrangement occurs upon guest removal in almost all cases.^{18,19} However no real effort has been made to study the exact physical mechanism of desolvation, partly because most systems were not suited for such a study. Although this realisation has been made serendipitously, the systems described in this chapter are very well suited for exploring these fundamental questions about guest desorption. In the case of **3**, the post-desorption phases are uniquely labelled ((*R*)-**1** or (*S*)-**2**) and furnish us with a means of confronting the process of desorption by studying molecular migration.

High resolution imaging was carried out using crystals of **2** and **3**. These studies were conducted using a Leo 1430VP Scanning Electron Microscope (SEM) equipped with a backscatter detector. All samples were coated with a thin layer of gold prior to analysis. Using a coupled on-line Link Energy Dispersive Spectroscopy (EDS) system, the instrument possesses the ability to differentiate between different elements present in selected regions of a micrograph. For the purposes of this study, it was particularly useful to differentiate between oxygen and sulphur, thus allowing differentiation between (*R*)-**1** and (*S*)-**2** phases.

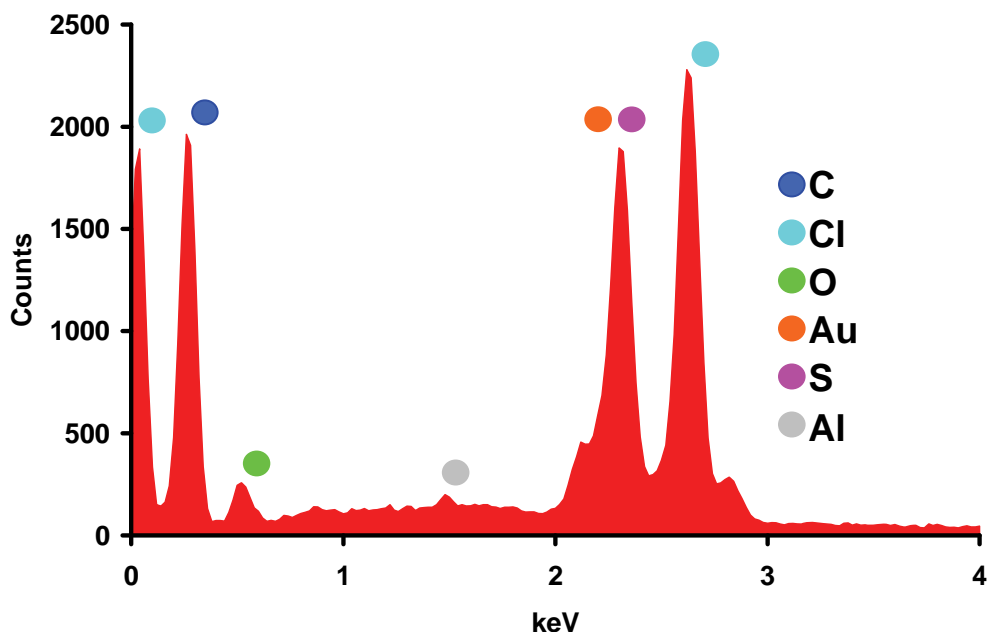


Figure 3.18 An EDS trace from a single crystal of 2_{CCl_4} showing the presence of the expected elements, as well as gold and aluminium, which are artefacts of the sample preparation.

Analysis of a single crystal of 2_{CCl_4} using the above-mentioned techniques revealed C, Cl, O and S to be present, as expected for the racemic carbon tetrachloride inclusion compound (Figure 3.18). A desorbed sample of 2_{CCl_4} was imaged (Figure 3.19) and analysed by EDS (Figure 3.20) to show large darker particles containing S, O and C (corresponding to pure **2**) and small lighter particles that were identified (owing to the presence of Cl) as some residual clathrate material.

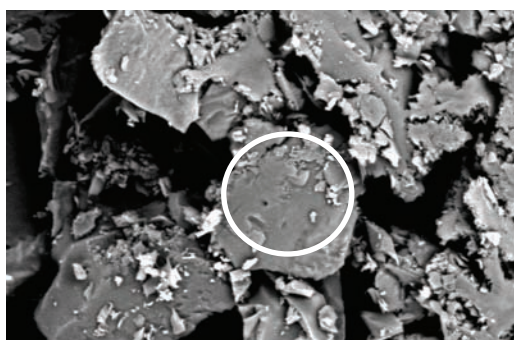


Figure 3.19 An electron micrograph of desorbed 2_{CCl_4} imaged using a backscatter detector which shows the contrast between the larger desorbed 2_{CCl_4} particles and the smaller solvent-containing 2_{CCl_4} particles. The white circle shows the location corresponding to the EDS measurement provided in Figure 3.20.

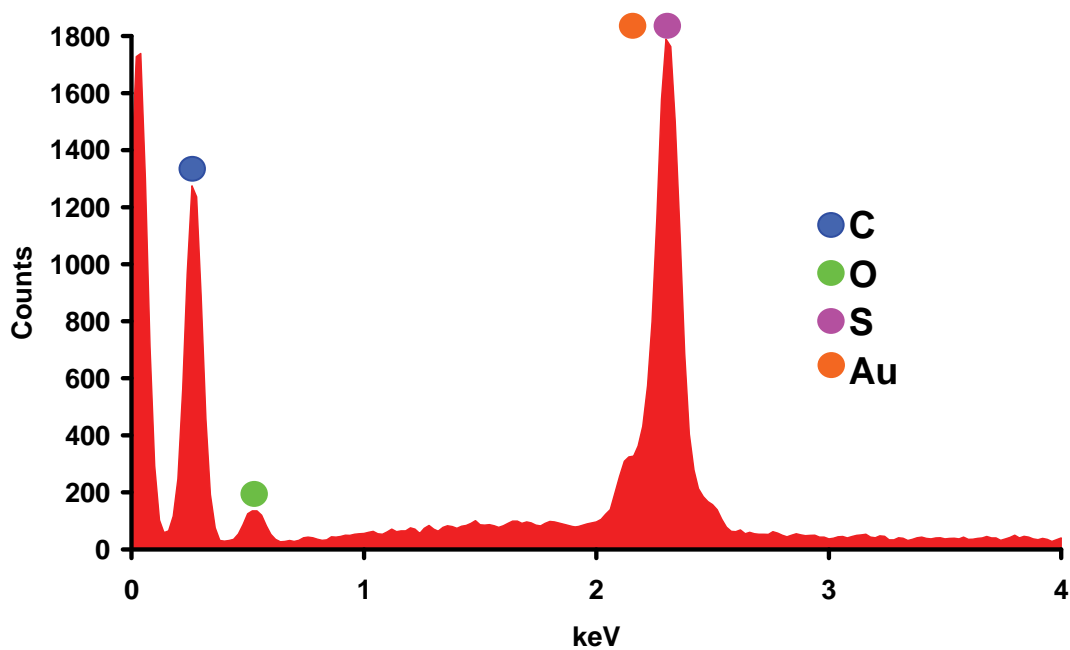
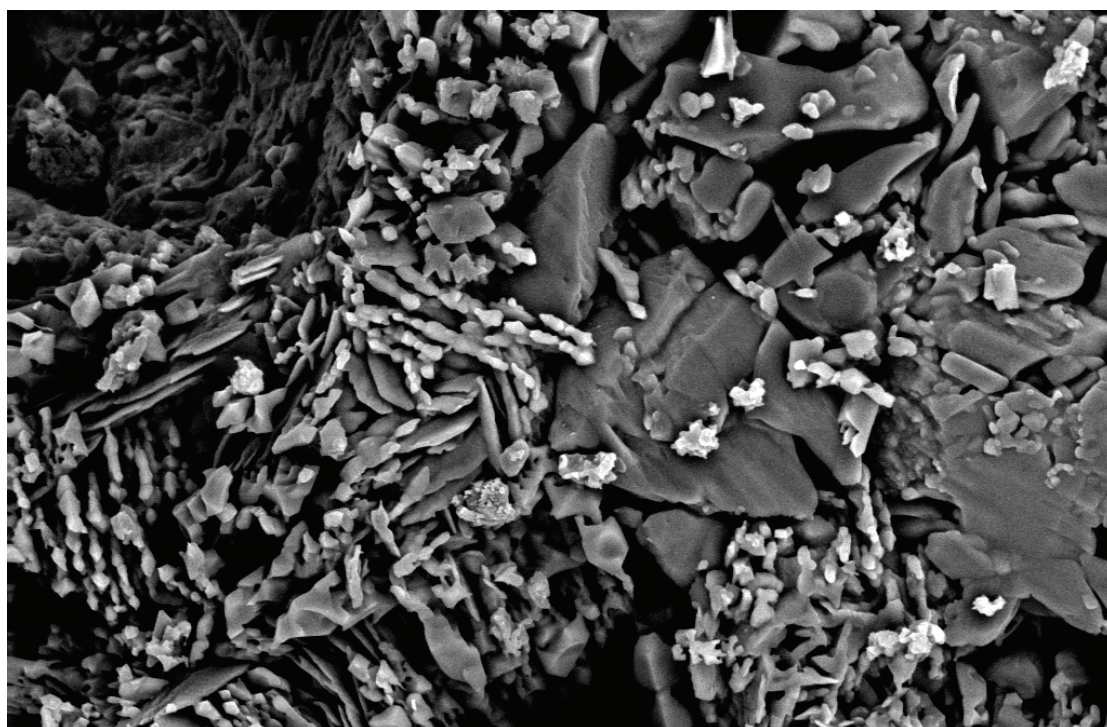


Figure 3.20 EDS analysis of desorbed 2_{CCl_4} , showing C, O and S present in the location circled in Figure 3.19.



20 μm

Figure 3.21 An electron micrograph of desorbed 3_{CCl_4} at 300x magnification showing that lighter regions (*i.e.* enriched with sulphur) and darker regions (containing only carbon and oxygen) are segregated as separate particles.

The micrograph of a desorbed sample of **3**_{CC14} shows the presence of two distinct particle morphologies (Figure 3.21). According to the EDS analysis, the larger darker particles are comprised exclusively of the (*R*)-**1** enantiomer (as indicated by the absence of sulphur, Figure 3.22) and the smaller lighter particles are recognised as the (*S*)-**2** enantiomer (as indicated by the distinct presence of sulphur, Figure 3.23). It is also interesting to note the difference in size of the two species – indeed, from XRPD analysis we inferred that resolved **1** is more crystalline than resolved **2** (Figure 3.16).

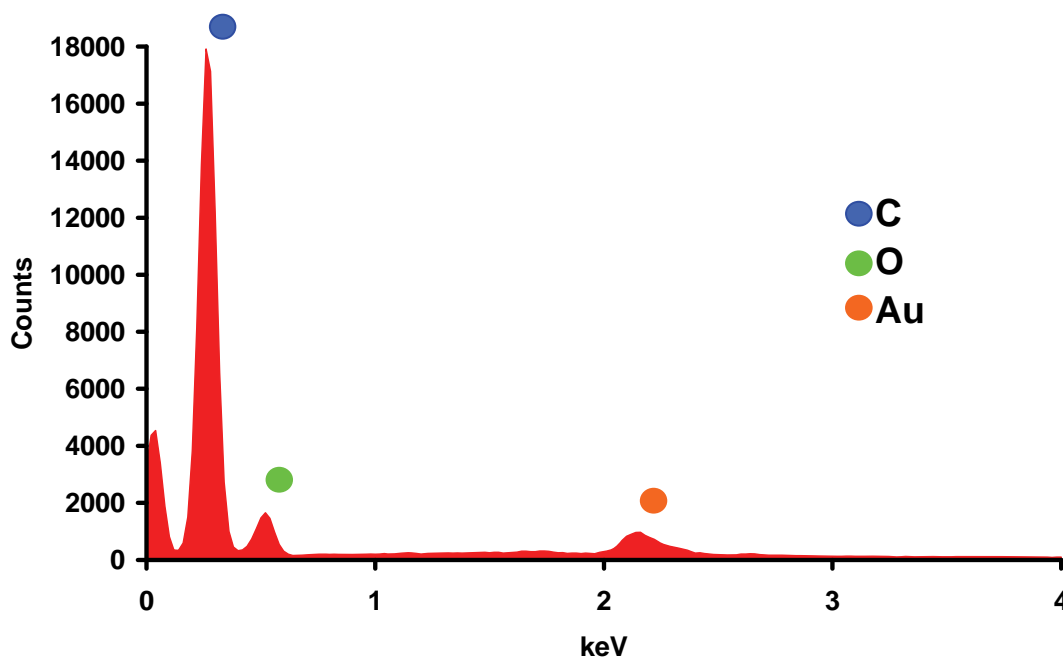


Figure 3.22 EDS trace of for the darker material in Figure 3.21. Owing to the absence of sulphur, this material is presumed to be (*R*)-**1**.

The results discussed above show that the (*R*)- and (*S*)-enantiomers segregate into separate and very distinct particles. It is tempting to argue that these observations are consistent with desolvation proceeding as a recrystallisation process rather than reorganisation. This study is not comprehensive enough to answer this question unequivocally, but it does serve to raise the right questions and to stimulate a more directed inquiry aimed at addressing this issue. After further studies it may even become apparent that phase-changes observed as a result of desolvation may result from a combination of the two processes, or that either process might occur, depending on the system. A logical starting point for such a study would be to conduct a literature survey to identify suitable systems for further investigation.

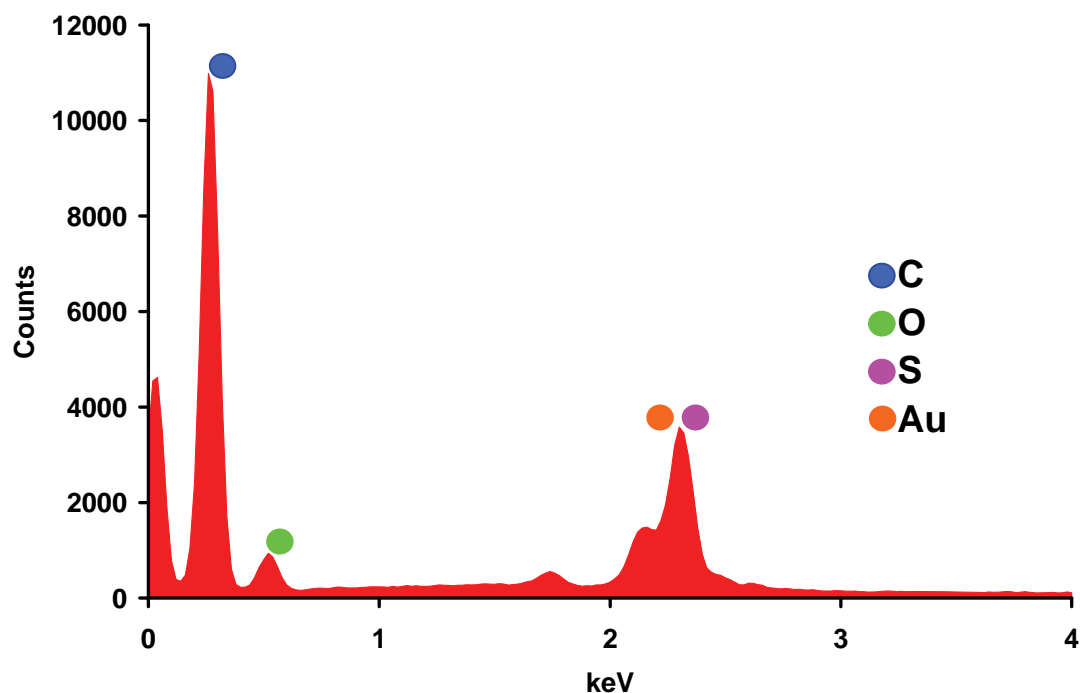


Figure 3.23 EDS trace for the lighter material in Figure 3.21. From the presence of sulphur, this material is presumed to be (S)-2.

3.2.4 Gas sorption

As mentioned above, the β_0 -phase of **1** can be prepared by subliming any clathrate of **1** with heating at reduced pressure. As discussed in 3.1, the affinity of this apparently porous material towards gases and vapours has been reported in two separate accounts.^{14,15} However, the assumption that the guests enter the lattice voids, was treated with caution and thus decided to revisit these findings. The results reported by Barrer seem to be at odds with conventional wisdom when considering the dimensions of the guests relative to that of the aperture between neighbouring lattice voids (Figure 3.6). We note that, while our own work also involves diffusion through seemingly nonporous media, it is possible in our case to postulate a mechanism based on thermal motion that does not seem feasible for Dianin’s compound. Furthermore, based on Barrer’s occupancy results, the packing efficiencies for the noble gases argon and xenon (assuming that these gases occupy the lattice voids as suggested) would be 0.81 and 0.91 respectively.[§] These are both in excess of the most efficient

[§] Using MSROLL, the volume of the cavity was determined as the volume accessible to a spherical probe with a radius corresponding to the van der Waals radius of the specific noble gas concerned.

close-packing arrangements of spheres (*i.e.* 0.74) in a regular arrangement as proved by Gauss (where 1.00 would be 100% efficient packing).

As part of this study, the β_0 -phase of **1** was exposed to N₂, CO₂ and H₂ using a gravimetric gas sorption instrument (described in section 2.5). Between 0 and 20 bar no sorption of N₂ or CO₂ was apparent at temperatures of 22, 0 and -40 °C (and also -80 °C in the case of CO₂). H₂ sorption experiments at 70, 22, 0, -40 and -80 °C revealed the possibility of a small interaction between host and guest, but this is not within the acceptable detection limits of the instrument and these results cannot therefore be quantified. Indeed, it is clear that H₂ sorption is negligible under the conditions used.

3.2.5 Serendipitous crystal engineering of polar order in a noncentrosymmetric host

The polar alignment of guests in a noncentrosymmetric space group has significance in the field of non-linear optics (NLO), and the exploitation of inclusion phenomena for such applications has received much attention.²⁰ Non-linear optical materials possess the specific property of second harmonic generation (SHG), which is of great interest for doubling the frequency of laser light.

Attempts based on the principles of crystal engineering have been made to create polar structures using hosts such as thiourea,²¹ tris-*o*-thymotide²² or racemic perhydrotriphenylene.¹⁷ Generally, the hosts form centrosymmetric structures and the strategy is to induce polarity in the crystals by ordering dipolar guests noncentrosymmetrically. Guests with high second-order molecular hyperpolarisabilities are preferred, but owing to electrostatics these often tend to form side-by-side head-to-tail dimers, ultimately resulting in centrosymmetric arrangements. The rationale behind using hosts with narrow channels is that these would facilitate in-line head-to-tail dipolar arrangements, especially within a given channel. This favourable structural feature would, however, be negated if neighbouring channels, though individually polar, align in an antiparallel fashion to once again produce an overall centrosymmetric structure. Another approach to potential SHG active materials is to use chiral host architectures such as urea, deoxycholic acids and β -cyclodextrin²³ (which might not be particularly polarisable

by themselves) to include appropriate guests such that the adduct exhibits NLO properties.²⁴ In the case of urea, the channel host has a strong propensity to order guest molecules in a unidirectional fashion.²¹

In this study, modification to one component of **1** (or **2**) resulted in the formation of a chiral host framework (**3**) that forces the majority of the carbon tetrachloride guests (which contain no net dipole moment, but are hyperpolarisable) to arrange in a one-dimensional head-to-tail fashion. Similar order is also imposed on the guests in neighbouring channels, which all arrange parallel with respect to one another along a polar axis. Since these crystals possess hyperpolarisable components that are aligned along the channel axis, *and* the overall structure is noncentrosymmetric, the material was expected to exhibit bulk SHG properties. Optical measurements were carried out on a single-crystal of **3**_{CCl₄}, and single crystals of compounds **1**_{CCl₄} and **2**_{CCl₄} were tested as control experiments. **3**_{CCl₄} displayed second harmonic generation for incident light of wavelength 780-820 nm (red laser) (Figure 3.24) while **1**_{CCl₄} and **2**_{CCl₄} showed no significant second harmonic response. The measurements were conducted using a tuneable red laser bundle focused using a short focal length lens ($f = 35$ mm). Radiation was then focused on the crystals which were oriented until the highest second harmonic signal was obtained. The average power of the second harmonic signal was measured (frequency-doubled to blue light at 400 nm) as a function of the average power of the incident fundamental wave. The experimental results clearly show that the effectiveness of second-harmonic conversion is low at small fundamental wave intensities, but is proportional to the increasing wave intensity, such that the power of the second-harmonic wave is proportional to the square of the fundamental intensity. This quadratic relationship is indicated by the fitted red line in Figure 3.24, but it can be observed that, at higher input power (>90 mW), this quadratic trend is no longer present. This is the result of saturation of the second harmonic generation process within the crystal.

No simple method exists for the quantification of second harmonic generation from single-crystal samples, since parameters such as crystal quality play a major role in precise measurements, and large crystals of sufficient optical quality are generally not accessible. However, experimental techniques for SHG quantification are available

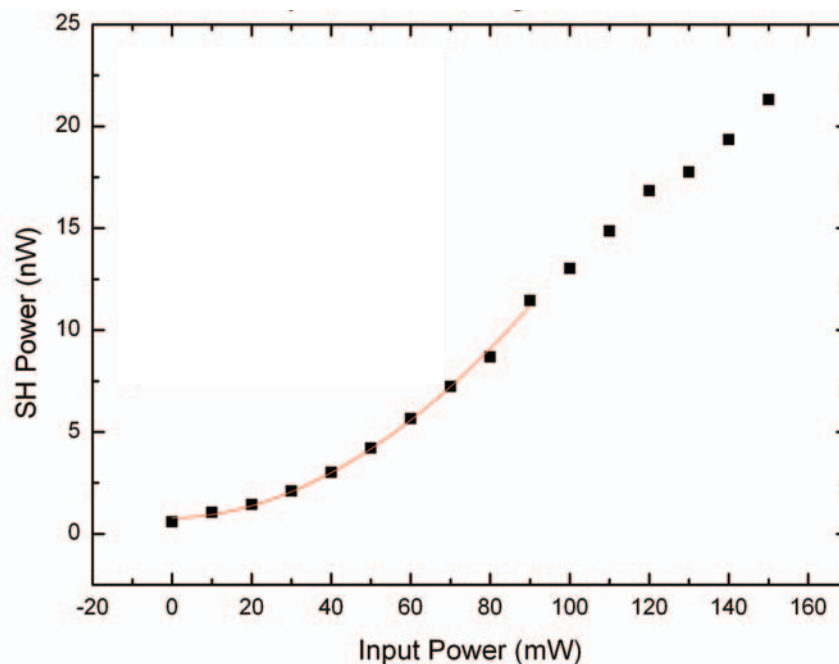


Figure 3.24 A plot showing the quadratic relationship between the input power of the fundamental wave (800 nm) and the measured intensity of the second harmonic wave at 400 nm as a fitted red line up to about 90 mW average input power.

for powders; samples can be sieved to reduce particle-size inconsistencies while the random orientation of particles serves to average out directional effects (in much the same way as for XRPD).²⁵ Future studies of **3** in this regard will involve constructing a device to measure second harmonic generation from powder samples. The inclusion behaviour of **3** will also be investigated with regard to dipolar guests that possess three-fold symmetry (*e.g.* trimethylsilyl chloride and trichloroacetonitrile).

3.3 CONCLUSION

In examining the structure of **1**, the most striking feature is the hexameric hydrogen bonded ring. After noting the ability of the compound to encapsulate guest molecules it was hypothesised that the ring is essential to its ability to form clathrates, and that the size of the ring would be critical to selectivity in sorption processes. Our initial aim was to alter one component of this hydrogen-donor acceptor adduct to thereby influence the ring size. It was anticipated that the different β_0 -phases would afford different guest selectivities and sorption profiles. Indeed, the “pore-size” of the clathrate was successfully engineered by combining one enantiomer of **1** with the opposite enantiomer of **2**. Unfortunately **2** and **3** could not be obtained in their empty

β_0 -forms for subsequent gas sorption and selectivity studies. Instead the results of this study presented a unique opportunity to study guest desorption and concomitant phase changes of clathrates **2**_{CCl₄} and **3**_{CCl₄}. These results raise some fundamental questions about the mechanisms of desolvation in organic inclusion compounds. A more detailed study, including quantitative work, will need to be conducted in this regard to address the questions posed by the preliminary results obtained thus far. Another by-product of the pore-size engineering experiment was the assembly of a new clathrate that possesses chirality and an asymmetrical cavity. This result is of significance in the field of crystal engineering of channel inclusion compounds as non-linear optical materials. Future studies can also be carried out to probe the selective inclusion behaviour of **3** (as a means of chiral separation) when crystallised from an enantiomeric mixture of guests.

With regard to the gas sorption ability of **1**, we are well-aware that the frameworks of molecular crystals are not necessarily rigid. Indeed, credit for this realisation should be given to Barrer *et al.*¹⁴ who made such a statement in reference to the sorption of a variety of guests by Dianin's compound. However, we now believe that Barrer's results were misinterpreted and Dianin's compound is not a member of the growing list of seemingly nonporous porous compounds. Therefore, Barrer made the correct statement, but perhaps for the wrong reasons.

3.3.1 General procedures and instruments

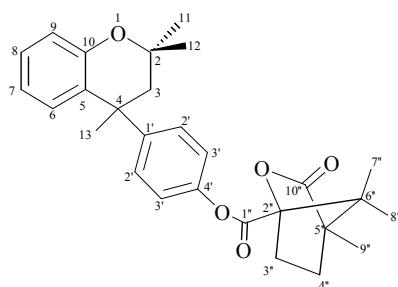
Dianin's compound **1** were prepared according to Baker *et al.*²⁶ Literature methods were adapted for the synthesis of compounds **2-12**.^{9,11,12} N,N'-dimethylformamide (DMF) was distilled over anhydrous MgSO₄ and dimethylthiocarbamoyl chloride was crystallised twice from petroleum-ether.

Melting points were determined on a TA Instruments Q100 differential scanning calorimeter or a Gallenkamp melting point apparatus, and are uncorrected. Mass spectra were recorded on an Agilent MSD 5975 GCMS instrument AMD 604 (EI+, 70 eV). NMR spectra were recorded on a Varian 300/400 FT or INOVA 600 MHz spectrometer (1H NMR at 300/400/600 MHz, 13C NMR at 75/100/150 MHz) with chemical shifts reported relative to an internal solvent resonance. The specific rotation for optically active substances was measured on a Bellingham and Stanley

Ltd. ADP220 polarimeter in spectroscopic grade ethanol. Optical rotations could not be determined for **4a**, **6a** and **8** since these materials crystallise from ethanol even at high dilution before measurements can be made. Owing to limited sample availability, a measurement of optical rotation for **10** could also not be obtained. Attenuated total reflection infrared spectroscopy was carried out on a Thermo Nicolet instrument using the Smart Golden Gate ATR attachment.

3.3.2 Synthesis and Characterisation

3.3.2.1 (*S,S*) and (*R,S*)-[*p*-(2,2,4-Trimethylchroman-4-yl)phenyl]camphanate (**4**)



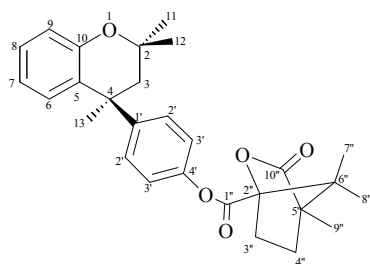
Dianin's compound (19.09 mmol, 5.371 g), DMAP (2.1 mmol, 256 mg) and triethylamine (60.24 mmol, 6.096 g) were dissolved in *ca* 70 mL dichloromethane. (1*S*)-(-)-camphanic chloride was then added (23.08 mmol, 5.00 g). The mixture was

stirred at room temperature for 27 hours to afford a clear orange solution, after which ice was added to quench the reaction. The aqueous phase was extracted with dichloromethane and the combined organic phases were washed with water, dried over MgSO₄ and the solvent removed under reduced pressure to afford an off-white solid material. Ethanol was added and the mixture refluxed. The flask was then cooled in an ice bath and the solution filtered to separate the white powder, which was washed with cold ethanol. The product was dried under vacuum for 3 hours.

Yield: 78.8%; M.p. 140.0-150.0 °C (Ethanol); δ_{H} (CDCl₃, 400 MHz) 0.924 (3H, s, H-12), 1.084 (3H, s, H-7"), 1.133 (3H, s, H-8"), 1.158 (3H, s, H-9"), 1.353 (3H, s, H-11), 1.713 (3H, s, H-13), 1.755 (1H, ddd, ²J = 13.1, ³J = 9.4, ⁴J = 4.2 Hz, H-4"en), 1.982 (1H, ddd, ²J = 13.2, ³J = 10.7, ⁴J = 4.4 Hz, H-4"ex), 2.095 (1H, d, ²J = 14.2 Hz, H-3 α), 2.180 (1H, ddd, ²J = 13.5, ³J = 9.3, ⁴J = 4.5 Hz, H-3"en), 2.374 (1H, d, ²J = 14.2 Hz, H-3 β), 2.547 (1H, ddd, ²J = 13.4, ³J = 11.0, ⁴J = 4.2 Hz, H-3"ex), 6.883 (1H, d, ³J = 8.3 Hz, H-9), 6.932 (1H, t, ³J = 7.3 Hz, H-7), 7.001 (2H, d, ³J = 8.6 Hz, H-3'), 7.173 (1H, t, ³J = 6.9 Hz, H-8), 7.186 (1H, d, ³J = 7.7 Hz, H-6), 7.230 (2H, d, ³J = 8.5 Hz, H-2'); δ_{C} (CDCl₃, 100 MHz) 9.72 (C-9"), 16.85 (C-7", C-8"), 27.44 (C-12), 27.46 (C-12), 28.97 (C-4"), 29.94 (C-11), 30.74 (C-3"), 32.41 (C-13), 32.43 (C-13), 39.19 (C-4), 50.30 (C-3), 54.65 (C-6"), 54.88 (C-5"), 74.51 (C-2), 90.83 (C-2"),

118.22 (C-9), 120.21 (C-7), 120.68 (C-3'), 127.46 (C-1'), 127.48 (C-1'), 127.95 (C-8), 128.14 (C-2'), 129.35 (C-6), 147.38 (C-4'), 148.33 (C-5), 148.36 (C-5), 153.58 (C-10), 166.10 (C-1"), 177.80 (C-10"); IR ν_{\max} (ATR, cm^{-1}) 2973 (sp^3 C-H stretch), 1791 and 1763 (C=O (ester) stretch), 1502 (C=C (aromatic) stretch), 1204, 1174 and 1053 (C-O stretch), 810 (out-of-plane C-H (para) aromatic bend), 760 (out-of-plane C-H (ortho) aromatic bend).

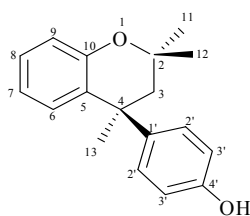
3.3.2.2 (S,S)-[p-(2,2,4-Trimethylchroman-4-yl)phenyl]camphanate (4a)



A diastereomeric mixture of Dianin-camphanoates (13.93 mmol, 6.25 g) was dissolved in a minimum of 2-methoxy-ethanol at 60 °C. Upon standing, white crystals formed, which were filtered and washed with methoxy-ethanol. The product was dried under high vacuum.

Yield: 28%; M.p. 180.7 °C (Methoxy-ethanol); $[\alpha]_{\text{D}}^{25.5} = -134.4 \pm 2.6^{\circ}$ (c=0.99, Benzene); δ_{H} equivalent to diastereomeric mixture (4); δ_{C} (CDCl_3 , 75.5 MHz) 9.72 (C-9"), 16.85 (C-7", C-8"), 27.47 (C-12), 28.97 (C-4"), 29.94 (C-11), 30.74 (C-3"), 32.45 (C-13), 39.19 (C-4), 50.30 (C-3), 54.65 (C-6"), 54.88 (C-5"), 74.51 (C-2), 90.83 (C-2"), 118.22 (C-9), 120.21 (C-7), 120.68 (C-3'), 127.49 (C-1'), 127.95 (C-8), 128.14 (C-2'), 129.35 (C-6), 147.83 (C-4'), 148.36 (C-5), 153.58 (C-10), 166.10 (C-1"), 177.80 (C-10").

3.3.2.3 (S)-4-p-Hydroxyphenyl-2,2,4-trimethylchroman (5)



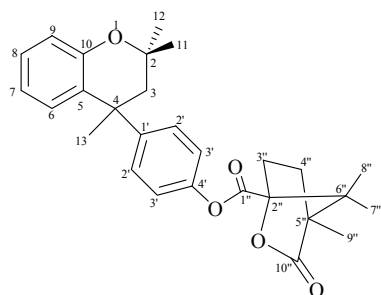
(S,S)-Dianin Camphanoate (3.34 mmol, 1.5 g) and sodium hydroxide (30.06 mmol, 1.20 g) were suspended/dissolved in a methanol/water (4:1) mixture. The reaction mixture was initially milky but clarified after some stirring. After an additional 2 hours of stirring, the methanol was removed under reduced pressure and this afforded a milky residue.

Water was added and the clear solution acidified (pH 2) to ensure protonation of the phenoxide. The aqueous mixture was extracted with three portions of dichloromethane, the combined organic phases dried over MgSO_4 and the solvent

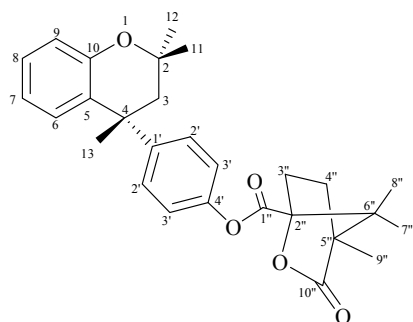
removed under reduced pressure. A milky white oil was afforded. The crude product was dissolved in a minimum of methanol under reflux and left for 2 days to crystallise. Trace amounts of (*R*)-DC were still present and clathrates formed. The crystals of racemic clathrates were removed by filtration and a few drops of water were added to the methanol mother liquor which now only contained the product (*S*)-DC. Upon slow evaporation of the solvent, colourless resolved DC crystals formed. The product was dried under high vacuum. These results were confirmed by determining the melting points of the racemic clathrates and the (*S*)-DC, respectively by differential scanning calorimetry.

Yield: 72.52%; M.p. 135.6-139.7 °C (Methanol/H₂O); $[\alpha]_D^{18.2} = -24.10^\circ$ (c=0.996, Ethanol); δ_H (CDCl₃, 300 MHz) 0.914 (3H, s, H-12), 1.344 (3H, s, H-11), 1.678 (3H, s, H-13), 2.059 (1H, d, ²J = 14.08 Hz, H-3 α), 2.347 (1H, d, ²J = 14.11 Hz, H-3 β), 4.940 (1H, s, OH), 6.701 (2H, td, ³J = 8.93, ⁴J = 2.19 Hz, H-3'), 6.871 (1H, dd, ³J = 8.35, ⁴J = 1.06 Hz, H-9), 6.925 (1H, td, ³J = 7.47, ⁴J = 1.29 Hz, H-7), 7.051 (2H, td, ³J = 8.83, ⁴J = 2.15 Hz, H-2'), 7.170 (1H, td, ³J = 8.55, ⁴J = 1.67 Hz, H-8), 7.198 (1H, dd, ³J = 7.42, ⁴J = 1.75 Hz, H-6); δ_C (CDCl₃, 75.5 MHz) 27.33 (C-12), 30.13 (C-11), 32.54 (C-13), 38.74 (C-4), 50.22 (C-3), 74.59 (C-2), 114.76 (C-3'), 118.04 (C-9), 120.03 (C-7), 127.69 (C-8), 128.07 (C-2'), 128.13 (C-1'), 129.37 (C-6), 142.37 (C-5), 153.33 (C-10), 153.58 (C-4'); MS (EI⁺) m/z 268 (M⁺), m/z 253 (100%, M⁺ - CH₃); IR ν_{max} (ATR, cm⁻¹) 3431 (O-H stretch (3257 broad band for rac-OH)), 3025 (sp² C-H stretch), 2977 and 2929 (sp³ C-H stretch), 1608 and 1511 (C=C (aromatic) stretch), 1381 and 1373 (CH₃ bend), 1196, 1178 and 1148 (C-O stretch), 836 (out-of-plane C-H (para) aromatic bend), 766 (out-of-plane C-H (ortho) aromatic bend).

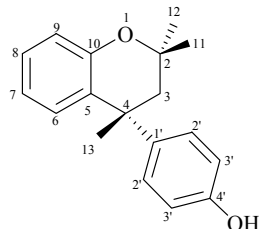
3.3.2.4 (*R,R*) and (*S,R*)-[*p*-2,2,4-Trimethylchroman-4-yl]phenyl]camphanate (6)



The same procedure was followed as for the synthesis of **4**, in this case (*1R*)-(+)-camphanic chloride was reacted with racemic **1**.

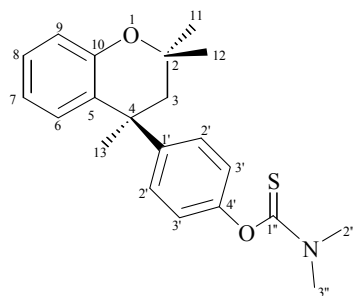
3.3.2.5 (R,R)-[*p*-2,2,4-Trimethylchroman-4-yl]phenyl]camphanate (6a)

The same procedure was followed as for the fractional crystallisation of **4a** from the diastereomeric mixture **4**. Owing to the limited amount of material available, the optical rotation could not be determined.

3.3.2.6 (R)-4-*p*-Hydroxyphenyl-2,2,4-Trimethylchroman) (7)

The chirally pure **7** was obtained in the same way as compound **5**.

M.p. 136.5-139.4 °C (Methanol); $[\alpha]_D^{19.1} = +25.15^\circ$
($c = 0.994$, Ethanol).

3.3.2.7 (S)-O-[*p*-(2,2,4-Trimethylchroman-4-yl)phenyl] Dimethylthiocarbamate (8)

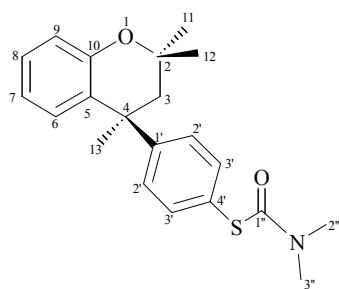
Sodium metal (2.74 mmol, 0.063 g) was dissolved in absolute ethanol and (*S*)-4-*p*-Hydroxyphenyl-2,2,4-trimethylchroman (2.39 mmol, 0.6422 g) was added to the solution. The reaction was carried out in an argon atmosphere. The solvent was removed under vacuum to produce the sodium phenoxide salt as a light orange glass. Dimethylthiocarbamoyl chloride (4.12 mmol, 0.51 g) dissolved in *N,N'*-dimethylformamide was added drop-wise to a solution of the Dianin phenoxide in the same solvent at 10 °C under a positive argon pressure. The reaction mixture was stirred for 1.5 hours at 40-45 °C. Upon cooling, the reaction mixture was added to water and extracted with benzene/hexane (4:1). The combined organic extracts were washed with water, 5% NaOH-, NaCl-solution (3x) and dried over MgSO₄. The organic layer was then filtrated and the solvent removed under reduced pressure to afford a yellow solid. The yellow solid was dissolved in a minimum volume of methanol and a few drops of benzene at 60 °C and recrystallised twice, washing each

time with cold methanol, to yield white crystals. The product was dried under vacuum. A small sample was re-dissolved in a minimum volume of methanol at room temperature and crystallised by slow evaporation to obtain cubic colourless crystals which were analysed by single crystal diffraction techniques.

Yield: 51.4%; M.p. 175.0-175.8 °C (Methanol); δ_{H} (CDCl_3 , 300 MHz) 0.949 (3H, s, H-12), 1.360 (3H, s, H-11), 1.739 (3H, s, H-13), 2.100 (1H, d, $^2J = 14.31$ Hz, H-3 α), 2.406 (1H, d, $^2J = 14.10$ Hz, H-3 β), 3.327 (3H, s, H-3''), 3.455 (3H, s, H-2''), 6.886 (1H, dd, $^3J = 8.09$, $^4J = 1.3$ Hz, H-9), 6.938 (2H, d, $^3J = 8.92$ Hz, H-3'), 6.938 (1H, td, $^3J = 8.08$, $^4J = 1.35$ Hz, H-7), 7.186 (1H, td, $^3J = 7.77$, $^4J = 1.66$ Hz, H-8), 7.216 (2H, d, $^3J = 8.71$ Hz, H-2'), 7.213 (1H, dd, $^3J = 7.67$, $^4J = 1.66$ Hz, H-6); δ_{C} (CDCl_3 , 75.5 MHz) 27.46 (C-12), 29.95 (C-11), 32.42 (C-13), 38.64 (C-3''), 39.15 (C-4), 43.22 (C-2''), 50.33 (C-3), 74.54 (C-2), 118.07 (C-9), 120.11 (C-7), 122.05 (C-3'), 127.69 (C-2'), 127.72 (C-1'), 127.79 (C-8), 129.49 (C-6), 147.53 (C-5), 151.84 (C-4'), 153.55 (C-10), 188.69 (C-1''); IR ν_{max} (ATR, cm^{-1}) 3025 (sp^2 C-H stretch), 2961 and 2926 (sp^3 C-H stretch), 1578 and 1498 (C=C (aromatic) stretch), 1348 (CH_3 bend), 1201 and 1128 (C-O stretch), 827 (out-of-plane C-H (para) aromatic bend), 766 (out-of-plane C-H (ortho) aromatic bend).

3.3.2.8 (S)-S-[p-(2,2,4-Trimethylchroman-4-yl)phenyl]

Dimethylthiocarbamate (9)



(S)-O-[p-(2,2,4-Trimethylchroman-4-yl)phenyl]

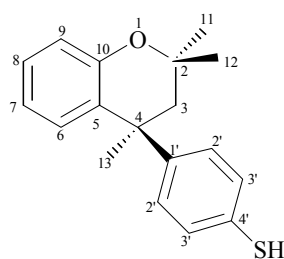
Dimethylthiocarbamate was placed in a glass tube to which a glass tap was attached. The sample was then evacuated and the tap closed off. Using a flame, the glass tube was then sealed under vacuum. The evacuated ampoule was heated at 270 °C for 5 hours in a Buchi

oven and the white crystals converted to a yellow gummy compound. Upon cooling, a colourless crystalline layer formed on top of the yellow sticky material, presumably unconverted **8** (in a previous experiment the heating step was only done for 1.75 hours and a lower yield of 46.85% was obtained). The sample was re-heated to 300 °C for another 4 hours and, upon cooling, only yellow material was visible inside the sealed glass vial. The ampoule was opened and the yellow compound was dissolved in CH_2Cl_2 and washed into a round bottomed flask. Flash chromatography was carried

out using silica gel (Art 9385 Kieselgel 60) with ethyl-acetate and petroleum-ether as eluant. Owing to the similar polarities of **5** (of which trace amounts are present), the starting material and the product ($R_f(\mathbf{5}) = 0.39$, $R_f(\mathbf{8}) = 0.48$ and $R_f(\mathbf{9}) = 0.33$ in 10% ethylacetate, petroleum-ether), gradient elution was used, starting with a 1% ethyl-acetate mixture and ending with a 50/50 ethyl-acetate, petroleum-ether solution. The desired fractions were combined and the solvent was removed under reduced pressure to afford a clear oil. The product was then dissolved and crystallised from petroleum-ether (ethanol-benzene used in literature for racemic product).⁹ It is also possible to selectively crystallise unconverted (*S*)-O-Dianin-thiocarbamate from MeOH. Crystals for X-ray diffraction were grown by slow evaporation of a petroleum-ether solution of **9**.

Yield: 71.2%; M.p. 84.7-84.4 °C (Petroleum-ether); $[\alpha]_D^{15.7} = +32.87^\circ$ (c=0.998, Ethanol); δ_H (CDCl_3 , 300 MHz) 0.949 (3H, s, H-12), 1.360 (3H, s, H-11), 1.722 (3H, s, H-13), 2.101 (1H, d, $^2J = 14.23$ Hz, H-3 α), 2.405 (1H, d, $^2J = 14.22$ Hz, H-3 β), 3.060 (6H, br s, H-2'' and H-3''), 6.889 (1H, dd, $^3J = 8.15$, $^4J = 1.57$ Hz, H-9), 6.932 (1H, td, $^3J = 7.630$, $^4J = 1.38$ Hz, H-7), 7.188 (1H, td, $^3J = 7.068$, $^4J = 1.40$ Hz, H-8), 7.194 (1H, dd, $^3J = 7.147$, $^4J = 1.70$ Hz, H-6), 7.238 (2H, d, $^3J = 8.80$ Hz, H-3'), 7.370 (2H, d, $^3J = 8.53$ Hz, H-2'); δ_C (CDCl_3 , 75.5 MHz) 27.42 (C-12), 29.85 (C-11), 32.35 (C-13), 36.88 (C-2'' and C-3''), 39.37 (C-4), 50.19 (C-3), 74.49 (C-2), 118.11 (C-9), 120.14 (C-7), 125.75 (C-4'), 127.41 (C-5), 127.60 (C-2'), 127.85 (C-8), 129.55 (C-6), 135.32 (C-3'), 151.36 (C-1'), 153.54 (C-10), 167.05 (C-1''); IR ν_{max} (ATR, cm^{-1}) 3025 (sp^2 C-H stretch), 2967 and 2920 (sp^3 C-H stretch), 1665 (C=O (amide) stretch), 1577 and 1486 (C=C (aromatic) stretch), 1389 (CH_3 bend), 1204 and 1089 (C-O stretch), 825 (out-of-plane C-H (para) aromatic bend), 760 (out-of-plane C-H (ortho) aromatic bend).

3.3.2.9 (*S*)-4-*p*-Mercaptophenyl-2,2,4-trimethylchroman (10)



(*S*)-S-[*p*-(2,2,4-Trimethylchroman-4-yl)phenyl]

Dimethylthiocarbamate was dissolved in methanol and upon the addition of 15 ml aq. 10% NaOH solution. The reaction mixture turned light orange and then milky white. The reaction was continually stirred for 2 days at 70 °C

under nitrogen and gradually turned clear. The mixture was allowed to cool to room temperature and was acidified to pH 2 using HCl. Upon acidification, a white precipitate formed, and the mixture was transferred to a separating funnel. The product was extracted three times with chloroform, the combined organic extracts washed once with water and dried using MgSO₄. After filtration the excess solvent was removed under reduced pressure to afford a yellow oil, which solidified partially on standing. Flash chromatography was carried out using silica gel (Art 9385 Kieselgel 60) ethyl-acetate:petroleum-ether (1:7). The fractions containing product ($R_f = 0.44$) were combined and the solvent removed under reduced pressure to afford a white powder. The white powder was then dissolved in a minimum of cyclohexane at 80 °C. After seeding, colourless crystals started to form. Crystals were filtered and washed with cold cyclohexane and dried under vacuum. Colourless plates suitable for single-crystal diffraction could be isolated from dichloromethane-cyclohexane.

Yield: 57.1%; M.p. 133.8-134.9 °C (Cyclohexane); δ_H (CDCl₃, 300 MHz) 0.916 (3H, s, H-12), 1.346 (3H, s, H-11), 1.675 (3H, s, H-13), 2.068 (1H, d, ²J = 14.16 Hz, H-3 α), 2.347 (1H, d, ²J = 14.17 Hz, H-3 β), 3.375 (1H, s, SH), 6.878 (1H, dd, ³J = 7.93, ⁴J = 1.10 Hz, H-9), 6.927 (1H, td, ³J = 7.57, ⁴J = 1.22 Hz, H-7), 7.071 (2H, d, ³J = 8.55 Hz, H-2'), 7.154 (2H, d, ³J = 8.30 Hz, H-3'), 7.166 (1H, dd, ³J = 7.57, ⁴J = 1.71 Hz, H-6), 7.179 (1H, td, ³J = 7.32, ⁴J = 1.71 Hz, H-8); δ_C (CDCl₃, 75.5 MHz) 27.41 (C-12), 30.01 (C-11), 32.37 (C-13), 39.06 (C-4), 50.09 (C-3), 74.52 (C-2), 118.15 (C-9), 120.12 (C-7), 127.48 (C-5 or C-4'), 127.51 (C-5 or C-4'), 127.75 (C-2'), 127.86 (C-8), 129.33 (C-6), 129.37 (C-3'), 147.91 (C-1'), 153.58 (C-10); MS (EI⁺) m/z 284 (M⁺), m/z 269 (100%, M⁺ - CH₃); IR ν_{max} (ATR, cm⁻¹) 3025 (sp² C-H stretch), 2974 and 2929 (sp³ C-H stretch), 2501 (S-H stretch), 1577 and 1483 (C=C (aromatic) stretch), 1384 (CH₃ bend), 1204 (C-O stretch), 1101 (C-O stretch), 827 (out-of-plane C-H (para) aromatic bend), 760 (out-of-plane C-H (ortho) aromatic bend).

3.3.2.10 O-[*p*-(2,2,4-Trimethylchroman-4-yl)phenyl] Dimethylthiocarbamate (11)

The same procedure was followed as for the synthesis of **6**. Crystals for single crystal diffraction were grown from methanol.

Yield: 57.57%; M.p. 141.9-144.7 °C (Methanol); Characterisation equivalent to **8**.

3.3.2.11 S-[*p*-(2,2,4-Trimethylchroman-4-yl)phenyl] Dimethylthiocarbamate (12)

The same procedure was followed as for the synthesis of **9**. The crude product (light yellow solid) was purified by flash chromatography (Art 9385 Kieselgel 60) by adsorbing the product onto silica gel and doing a gradient elution starting with a 7% ethyl-acetate, petroleum-ether mixture and increasing the polarity gradually to 20% ethyl-acetate content. The product was obtained as a white crystalline solid ($R_f = 0.36$, 15% Ethyl-acetate, petroleum-ether). The material was recrystallised from ethanol-benzene to afford light yellow crystals. Unconverted **11** was also recovered after chromatography ($R_f = 0.48$, 15% Ethyl-acetate:petroleum-ether). The product was dried under vacuum. A small amount of material was redissolved in methanol, and slow evaporation yielded crystals suitable for single crystal diffraction.

Yield: 96.43%, M.p. 124.4-126.5 °C; Characterisation equivalent to **9**.

3.3.2.12 4-*p*-Mercaptophenyl-2,2,4-trimethylchroman (2)

The same procedure was followed as for the synthesis of **10**. Crystals of the racemic clathrate suitable for single crystal diffraction were grown from carbon tetrachloride.

Yield: 75.23%; M.p. 105.8-109.6 °C (Carbon tetrachloride); Characterisation equivalent to **10**.

REFERENCES

- 1 A. P. Dianin, *J. Russ. Phys. Chem. Soc.* **1914**, *31*, 1310-1319.
- 2 W. Baker, J. F. W. McOmie, *Chem. Ind.* **1955**, 256.
- 3 H. M. Powell, B. D. P. Wetters, *Chem. Ind.* **1955**, 256-257.
- 4 W. Baker, A. J. Floyd, J. F. W. McOmie, G. Pope, A. S. Weaving, J. H. Wild, *J. Chem. Soc. Abstr.* **1956**, 2010-2017.
- 5 J. L. Flippen, J. Karle, I. L. Karle, *J. Am. Chem. Soc.* **1970**, *92*, 3749-3755.
- 6 F. Imashiro, M. Yoshimura, T. Fujiwara, *Acta Crystallogr., Sect. C: Cryst. Struct. Commun.* **1998**, *54*, 1357-1360.
- 7 A. D. U. Hardy, D. D. MacNicol, J. J. McKendrick, D. R. Wilson, *Tetrahedron Lett.* **1975**, 4711-4712.
- 8 A. D. U. Hardy, D. D. MacNicol, J. J. McKendrick, D. R. Wilson, *J. Chem. Soc., Chem. Commun.* **1977**, 292-293.
- 9 A. D. U. Hardy, J. J. McKendrick, D. D. MacNicol, D. R. Wilson, *J. Chem. Soc., Perkin Trans. 2* **1979**, 729-734.
- 10 T. Jacobs, M. W. Bredenkamp, E. J. C. de Vries, *Acta Crystallogr., Sect. E: Struct. Rep. Online* **2007**, *63*, 03736-U02368.
- 11 M. J. Brienne, J. Jacques, *Tetrahedron Lett.* **1975**, 2349-2352.
- 12 C. Esterhuysen, M. W. Bredenkamp, G. O. Lloyd, *Acta Crystallogr., Sect. C: Cryst. Struct. Commun.* **2005**, *61*, O32-O34.
- 13 G. O. Lloyd, M. W. Bredenkamp, *Acta Crystallogr., Sect. E: Struct. Rep. Online* **2005**, *61*, O1512-O1514.
- 14 R. M. Barrer, V. H. Shanson, *J. Chem. Soc., Chem. Commun.* **1976**, 333-334.
- 15 K. J. Harrington, C. P. Garland, *Sep. Sci. Technol.* **1982**, *17*, 1339-1349.
- 16 A. Collet, J. Jacques, *Isr. J. Chem.* **1977**, *15*, 82-83.
- 17 O. Konig, H. B. Burgi, T. Armbruster, J. Hulliger, T. Weber, *J. Am. Chem. Soc.* **1997**, *119*, 10632-10640.
- 18 L. J. Barbour, M. R. Caira, A. Coetzee, L. R. Nassimbeni, *J. Chem. Soc., Perkin Trans. 2* **1995**, 1345-1349.
- 19 M. R. Caira, A. Coetzee, L. R. Nassimbeni, F. Toda, *J. Chem. Res., Synop.* **1996**, 280-281.
- 20 K. D. M. Harris, J. M. Thomas, *J. Chem. Soc., Faraday Trans.* **1990**, *86*, 2985-2996.
- 21 K. D. M. Harris, *Chem. Soc. Rev.* **1997**, *26*, 279-289.
- 22 W. Tam, D. F. Eaton, J. C. Calabrese, I. D. Williams, Y. Wang, A. G. Anderson, *Chem. Mater.* **1989**, *1*, 128-140.
- 23 S. Tomaru, S. Zembutsu, M. Kawachi, M. Kobayashi, *J. Chem. Soc., Chem. Commun.* **1984**, 1207-1208.

- 24 D. F. Eaton, A. G. Anderson, W. Tam, Y. Wang, *J. Am. Chem. Soc.* **1987**, *109*, 1886-1888.
- 25 S. K. Kurtz, T. T. Perry, *J. Appl. Phys.* **1968**, *39*, 3798-3813.
- 26 W. Baker, J. F. W. McOmie, A. S. Weaving, *J. Chem. Soc. Abstr.* **1956**, 2018-2020.

CHAPTER 4

METALLOCYCLES

4.1 INTRODUCTION

It is well-known that crystalline materials consist of atoms, molecules or ions that pack closely such that interstitial voids larger than 25 \AA^3 do not occur readily.¹ However, since synthetic materials with sub-nanometre scale pores and cavities are of considerable interest for the separation, storage and sensing of gases,² much effort has been devoted to countermanding close-packing tendencies to thereby engineer and even tune empty space in crystals.^{3,4} In recent years the vast majority of this research has been devoted to studies of crystalline coordination compounds. This can partly be ascribed to the great structural diversity arising from different transition metal coordination geometries and the variety of multidentate ligands available to build supermolecules. Indeed, transition-metal-based supermolecules have already shown much promise with potential applications including molecular recognition,⁵ chiral recognition⁶ and catalysis.^{7,8} It is anticipated that continued research efforts will in due course lead to new materials with tuneable properties.

The coordination-driven motif offers an easier alternative to the synthesis of discrete supramolecular units, this is in contrast to classic syntheses involving covalently bound macromolecules.⁹ Despite continuous efforts to predict and define the parameters governing the assembly of zero-dimensional (0D), discrete architectures¹⁰ of coordination compounds, the rational design of such structures is not always possible. More information about *chiral* metallocycles and their specific applications is given in a recent review by Lin.¹¹ For an up-to-date review of the assembly of metallocyclic supermolecules for molecular recognition and sensing, the recent article by Sun and Lees can be consulted.⁵ Our approach to the construction of porous materials is to utilise cyclic host molecules or complexes that are shape-incompatible and cannot therefore interdigitate to form close-packed structures.^{12,13} Thus, even when efficiently packed in the crystalline state, these structural motifs are predisposed to yield significant solvated space or voids in the structure. Previous attempts by our

group to design molecules with this topology have been successful twice.¹²⁻¹⁴ Figure 4.1 shows a rectangular complex assembled from two silver ions bridged by two 1,4-bis-(2-methylimidazol-1-ylmethyl)benzene molecules coordinating *exo-bidentately* *via* the imidazole groups. These ring complexes stack to form channels encapsulating acetonitrile guest molecules, which can be removed by heating the crystals to $> 80^{\circ}\text{C}$ to produce an empty porous host.

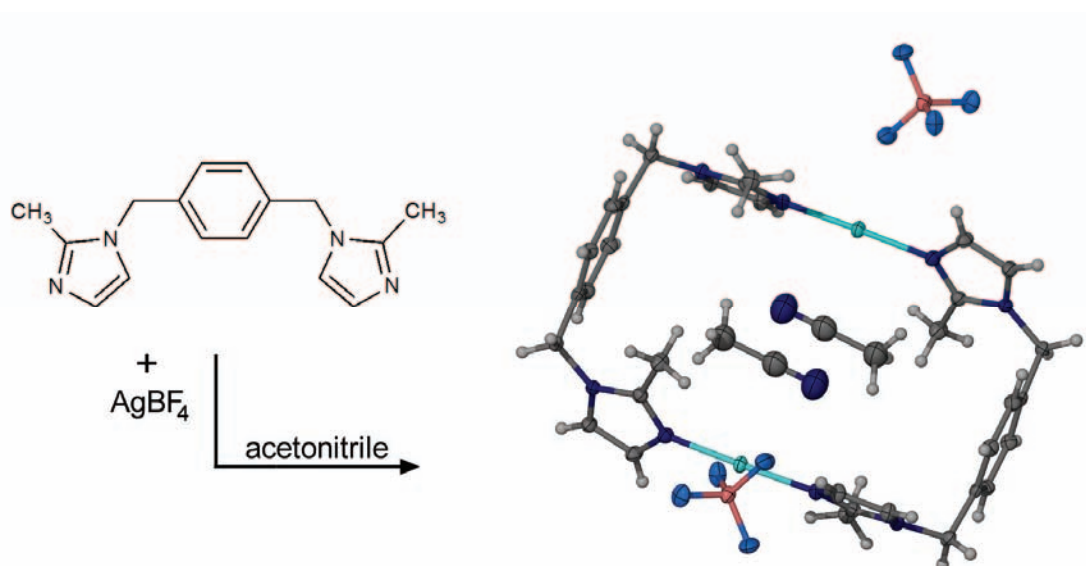


Figure 4.1 Formation of $[\text{Ag}_2(1,4\text{-bis}(2\text{-methylimidazol-1-ylmethyl)-benzene})_2](\text{BF}_4)_2 \cdot 2\text{CH}_3\text{CN}$.¹²

In the second instance, the ligand 1,3-bis(imidazolyl-1-ylmethyl)-2,4,6-trimethylbenzene was reacted with $\text{CuCl}_2 \cdot \text{H}_2\text{O}$ to form a discrete metallocycle (Figure 4.2) reminiscent of the silver-metalloporphyrin. However, in this case each metal ion is coordinated in an irregular tetrahedral fashion to the imidazole moieties as well as the chloride anions. These molecules also stack linearly, but form discrete voids, each containing a single water molecule as well as a methanol molecule. Single-crystal diffraction and thermal analysis studies showed that the guest molecules could also be removed to produce an empty host lattice. Permeability of the material to gases such as nitrogen, carbon monoxide, methane and carbon dioxide has been demonstrated.¹³ A molecular mechanics simulation (unpublished results) suggests that 1D diffusion occurs during which carbon dioxide molecules are transferred from one cavity to another within a stacked column.*

* Further information on the molecular mechanics simulation is available from Prof J. Dillen of the Department of Chemistry and Polymer Science at the University of Stellenbosch.

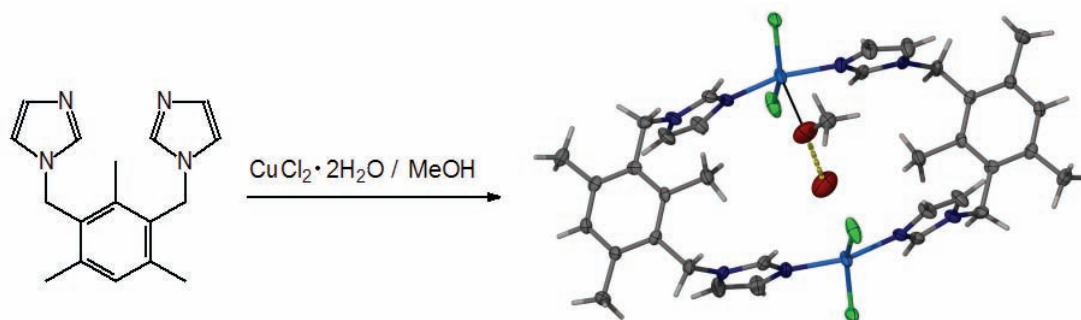
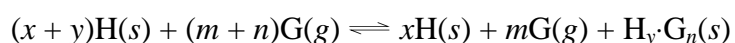


Figure 4.2 Formation of $[\text{Cu}_2(1,3\text{-bis(imidazol-1-ylmethyl)-2,4,6-trimethylbenzene})_2\text{Cl}_4] \cdot \text{CH}_3\text{OH} \cdot \text{H}_2\text{O}$.¹³

Remarkably, in both cases described above, the single crystals survive guest-removal without significant loss of mosaicity. While this phenomenon is not important for guest sorption/desorption processes, it is of substantial value with regard to our ability to characterise the material using single-crystal diffraction methods.

Four novel ligands have been prepared as part of the present study, namely 4,4'-bis(benzimidazol-1-ylmethyl)biphenyl,¹⁵ 4,4'-bis(2-methylbenzimidazol-1-ylmethyl)biphenyl, 1,4-bis(2-methylimidazolyl)-2-butyne and 4,4'-bis(2-methylimidazol-1-ylmethyl)biphenyl (Figure 4.3). The common theme in this series of ligands is that they all consist of two imidazole-derived coordinating groups separated by a rigid spacer. To date, coordination compounds prepared from the first three ligands have not yielded porous materials and further discussion will be limited only to compounds containing 4,4'-bis(2-methylimidazol-1-ylmethyl)biphenyl (**L**, Figure 4.3c). On complexation of **L** with cobalt, zinc and cadmium (*i.e.* the chloride salts of the divalent metal), the ligand assumes a C-shaped conformation to form a series of discrete neutral molecular “hexagons.” These “hexagons” are dinuclear $[\text{M}_2\text{L}_2\text{Cl}_4]$ complexes that stack to form columns in the solid state. It has been shown that such rings are solvent-templated, and that the nature of the solvent influences the overall conformation of the complex.¹⁶

Much of the effort within our group is aimed at the construction of porous materials. As previously mentioned, such materials have potential applications for the sorption of gas and possible separation of gaseous mixtures. The process of gas uptake/release can conveniently be represented by the reaction equation:



where H is the empty host, G the gaseous guest and $H_y \cdot G_n$ the host:guest complex.

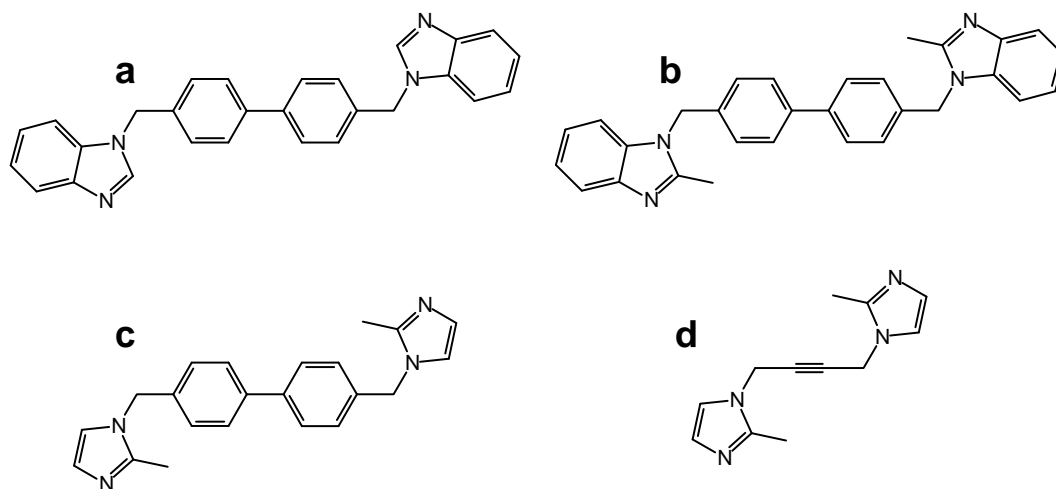
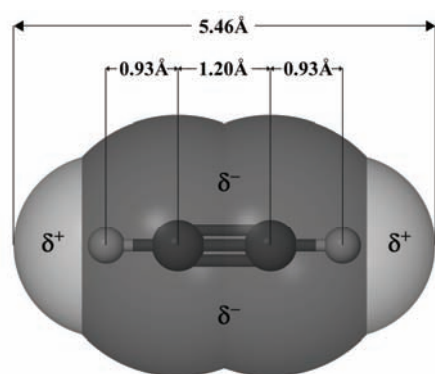


Figure 4.3 (a) 4,4'-bis(benzimidazol-1-ylmethyl)biphenyl, (b) 4,4'-bis(2-methylbenzimidazol-1-ylmethyl)biphenyl, (c) 4,4'-bis(2-methylimidazol-1-ylmethyl)biphenyl and (d) 1,4-bis(2-methylimidazolyl)-2-butyne.

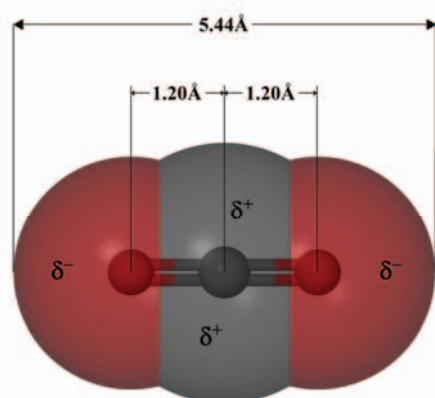
Upon exposure of the initially empty host crystals $(x+y)H$ to the gaseous guest $(m+n)G$, sorption begins and some of the guest is incorporated into the host to yield $H_y \cdot G_n$. The forward reaction is kinetically controlled until the three phases H, G and $H_y \cdot G_n$ reach their equilibrium states. Under equilibrium conditions at a given temperature, the composition of the $H_y \cdot G_n$ adduct will depend on the overpressure of the gas G. Thus, the determination of the structure of $H_y \cdot G_n$ by diffraction methods poses a non-trivial practical challenge, *i.e.* the material must be exposed to a constant (preferably known) pressure of the relevant gas during the entire process of intensity data collection. There is an urgent need to address this challenge by means of a practical method that can be applied in a conventional single-crystal X-ray diffraction laboratory. Takamizawa has used a method that involves sealing a crystal into a thick-walled glass capillary together with a solid or liquid guest (*i.e.* CO_2 , CH_4 , O_2 or Ar) obtained by condensation of the latter in a liquid nitrogen bath.¹⁷⁻¹⁹ After equilibrating the capillary to room temperature, the pressure of the gas is approximated by estimating the volumes of the capillary and of the condensed gas. Other single-crystal diffraction experiments²⁰⁻²⁴ have been conducted by sealing porous crystals in capillaries together with various gases or vapours at relatively low pressures (approximately one atm). The above-mentioned experiments have yielded

valuable information about guest binding sites, but the exact pressure (which we know to have a direct influence on the loading) at which these structures were determined is unknown. These methods are not suitable for the accurate control of pressure, or for conducting a systematic series of measurements with the same crystal exposed to different pressures. Such experiments can, however, be conducted using powder diffraction methods and employing synchrotron radiation,²⁵⁻²⁸ but this is a highly specialised process requiring facilities that are not readily accessible. Furthermore, Rietveld refinement methods are generally not comparable to those employed for single crystals with regard to difference electron density mapping and modelling disorder of either the host framework or positions of guest molecules, and information about subtle host:guest interactions may therefore be limited. As part of this study we developed a simple, inexpensive method for collecting single-crystal X-ray data of a crystal under known and accurately controllable gas pressures using a conventional X-ray diffractometer. The simplicity of this system facilitates incremental increase of the gas pressure between successive data collections and ultimately provides unprecedented structural detail with regard to the progression of the sorption process.

The sensitivity of our method was demonstrated using acetylene and carbon dioxide - two gases with similar dimensions and boiling points, but contrasting electrostatic profiles (Figure 4.4). Sorption studies reveal subtle differences in the uptake of these two gases by the seemingly nonporous material possessing void spaces that are each capable of accommodating up to two gas molecules. A series of equilibrium structures at systematically controlled pressures of C₂H₂ illustrates the step-wise uptake of the gas. The level of structural detail obtained from this study using the new gas cell cannot be matched by other existing methods. The differences in sorption behaviour between C₂H₂ and CO₂ can also be rationalised on the basis of host:guest interactions at play during the uptake process. With this method, valuable insight into the equilibrium interactions between solid hosts and gaseous guests could be obtained in a conventional X-ray diffraction laboratory, and the influence of pressure can be quantified.

**Acetylene**

boiling point = $-84.7\text{ }^{\circ}\text{C}$
 molecular volume = $33.4\text{ }\text{\AA}^3$

**Carbon dioxide**

boiling point = $-78.5\text{ }^{\circ}\text{C}$
 molecular volume = $33.9\text{ }\text{\AA}^3$

Figure 4.4 Idealised^{†29-31} van der Waals representations of acetylene and carbon dioxide.

The volumetric gas sorption apparatus and the pressure cell for single-crystal data collection are described in sections 2.6 and 2.7 and the design, synthesis and structures of the potential porous crystalline materials are discussed in the present chapter. In each case, details of the preparation of the β_0 -phases are given, followed by porosity studies. Finally, with the aid of high quality single-crystal data of host:guest interactions, thermodynamic data of the sorption process and statistical mechanics calculations, a possible gas transport mechanism is discussed. Observations about the impact on the host lattice with increased loading are discussed, along with the influence of different guests with regard to adsorbate-adsorbate and adsorbent-adsorbate interactions.

[†] Idealised geometry is based on the following assumptions:

van der Waals radii: Carbon = $1.70\text{ }\text{\AA}$ Hydrogen = $1.20\text{ }\text{\AA}$ Oxygen = $1.52\text{ }\text{\AA}$
Bond lengths: C-H = $0.93\text{ }\text{\AA}$ C≡C = $1.20\text{ }\text{\AA}$ C=O = $1.20\text{ }\text{\AA}$

4.2 RESULTS AND DISCUSSION

4.2.1 Solvent-templated self-assembly: a single-crystal study

The ligand 4,4'-bis(2-methylimidazol-1-ylmethyl)biphenyl (**L**) was synthesised (see section 4.4.1.1) and a series of discrete dinuclear metallocycles with general formula $[M_2L_2X_4]$ were prepared, each containing a different metal cation (M), halide anion (X) and guest solvent (Figure 4.5). Compound **13**_{MeOH} was prepared by layering dilute equimolar solutions of $CoCl_2 \cdot 6H_2O$ in $CHCl_3$ and **L** in MeOH and allowing the layers to mix slowly by diffusion. The subscript adjacent to the compound number (MeOH in this case) denotes the guest species encapsulated within each compound. Analogously, **14**_{MeOH} was prepared using $ZnCl_2$, **15**_{MeOH} using $CdCl_2 \cdot 2.5H_2O$ and **17**_{MeOH} using $CdBr_2 \cdot 4H_2O$; in every case the metal salt was dissolved in methanol and **L** in chloroform. Using CdI_2 , compound **16**_{CHCl₃} was prepared in the same way as the methanol solvates (**13**_{MeOH}, **14**_{MeOH}, **15**_{MeOH} and **17**_{MeOH}), but in this case the metallocycle preferentially included chloroform. Compound **16**_{CH₂Cl₂} was formed by diffusion mixing of **L** in MeCN with the metal salt (CdI_2) in dichloromethane. The product was once again shown to selectively include the chlorinated solvent. Each of these coordination reactions yielded crystals suitable for single-crystal X-ray diffraction.

Structure elucidation (**13-17**_{guest}) revealed isostructural discrete metallocycles, all of which crystallised in the monoclinic space group $C2/m$. Each complex is composed of two metal ions that are tetrahedrally coordinated to two halide anions and two bridging ligands. The resulting cyclic complexes (Figure 4.5) are stacked along the crystallographic *c*-axis as shown in Figure 4.6.

Compound **13**: $\text{CoCl}_2 \cdot 6\text{H}_2\text{O}$

Compound **14**: ZnCl_2

Compound **15**: $\text{CdCl}_2 \cdot 2.5\text{H}_2\text{O}$

Compound **16**: CdI_2

Compound **17**: $\text{CdBr}_2 \cdot 4\text{H}_2\text{O}$

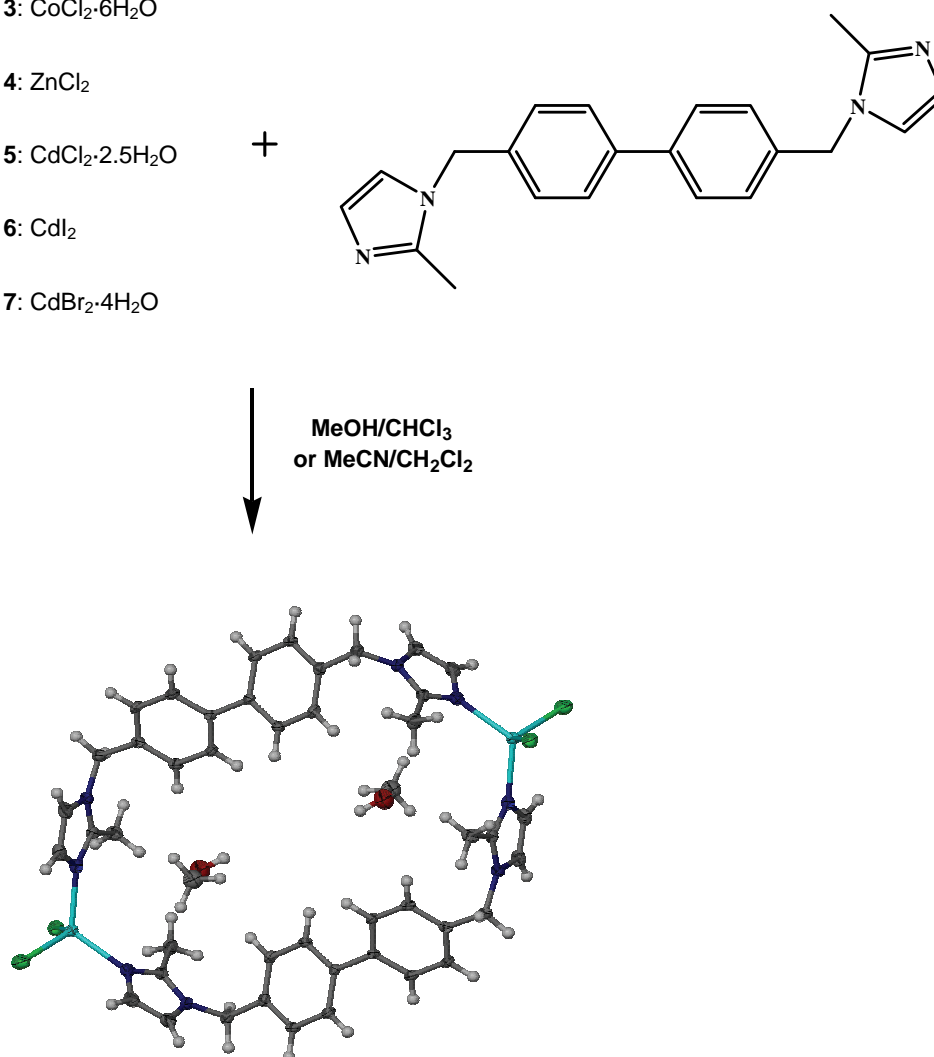


Figure 4.5 Scheme showing the formation of $[\text{Co}_2\text{L}_2\text{Cl}_4] \cdot 2\text{MeOH}$ (**13_{MeOH}**), $[\text{Zn}_2\text{L}_2\text{Cl}_4] \cdot 2\text{MeOH}$ (**14_{MeOH}**), $[\text{Cd}_2\text{L}_2\text{Cl}_4] \cdot 2\text{MeOH}$ (**15_{MeOH}**) and $[\text{Cd}_2\text{L}_2\text{Br}_4] \cdot 2\text{MeOH}$ (**17_{MeOH}**). The metallocycles of $[\text{Cd}_2\text{L}_2\text{I}_4] \cdot \text{CHCl}_3$ (**16_{CHCl3}**) and $[\text{Cd}_2\text{L}_2\text{I}_4] \cdot \text{CH}_2\text{Cl}_2$ (**16_{CH2Cl2}**) are isostructural to that depicted here.

Figure 4.6 shows how the metallocycles (numbered one to four) of **13-15_{MeOH}** enclose two methanol molecules each. This packing mode creates a solvent-filled pocket between two adjacent metallocycles and each metallocycle shares a cavity with both of its neighbouring metallocycles (*i.e.* a solvent-filled cavity exists between metallocycles 2 and 3, but also between metallocycles 1 and 2, and metallocycles 3 and 4). The ends of the approximately rectangular pocket are bounded by the chloride ions, while the phenyl and methyl hydrogen atoms of **L** form the walls of the cavity, *i.e.* chloride anions of metallocycles 1 and 4 (shown space-filled) stopper the top and bottom of a cavity while the sides are formed by the van der Waals surfaces of

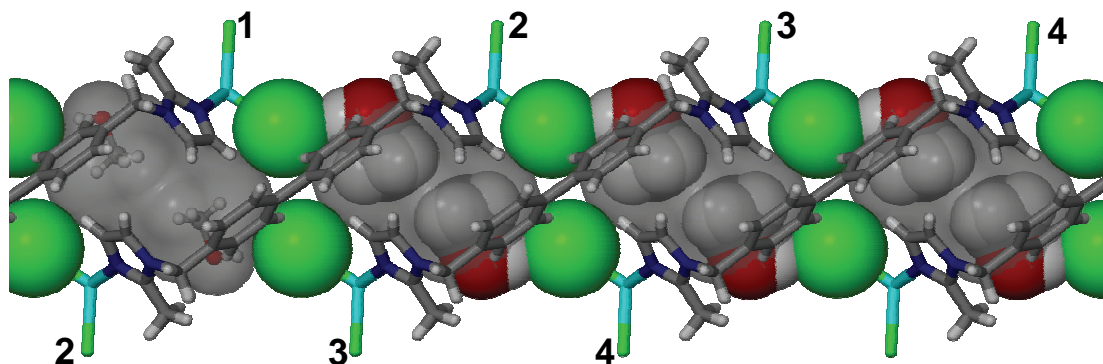


Figure 4.6 The metalocycles encapsulating guest molecules viewed along [010]. The neutral complexes are shown as capped-sticks and the guest molecules are shown in ball-and-stick in the left-most cavity and van der Waals representation in the remaining cavities. Connolly surfaces (using a probe radius of 1.4 Å) of the solvent-filled pockets are shown in semi-transparent grey. The host metalocycles [$M_2L_2Cl_4$, where $M = Co$ (**13**), Zn (**14**), or Cd (**15**)] enclathrates two methanol molecules per cavity with mapped volumes increasing from 118 to 124 to 131 Å³, respectively, for **13**_{MeOH}, **14**_{MeOH} and **15**_{MeOH}.

metalocycles 2 and 3. The methanol molecules are presumed to template the assembly of the molecular hexagons and two chloride anions of every metalocycle form O–H···Cl[−] hydrogen bonds with two solvent molecules: $D\cdots A = 3.203(6)$, $3.186(9)$ and $3.173(5)$ Å for **13–15**_{MeOH}, respectively. The metalocycles and methanol guests for all of these structures are located about sites of $2/m$ symmetry, with a mirror plane running parallel to the projection plane of Figure 4.6 and passing through the metal centres. In the case of **13**_{MeOH}, the calculated position of the hydroxyl hydrogen atom is on the mirror plane. For **15**_{MeOH} the hydrogen atom was placed on the mirror plane and refined freely with a loose restraint on the O–H distance; an acceptable standard uncertainty was obtained in this manner. For **14**_{MeOH} the hydroxyl hydrogen atom was also placed on the mirror plane, but the O–H···Cl geometry needed to be constrained in order to keep it there during refinement. Using this procedure, nonsensical standard uncertainties were obtained, and it was thus necessary to use a calculated model that requires an equal occupancy disorder of the hydrogen atom on either side of the (010) mirror plane. In considering the O–H···Cl[−] angle, excellent directionality is implied for the hydrogen bonds in both **13**_{MeOH} and **15**_{MeOH} with $\angle DHA = 175.8^\circ$ and $175(9)^\circ$, respectively. For **14**_{MeOH} this is not the case since the O–H bond and the H···Cl[−] interactions are not in the ac plane. In the disordered model, $\angle DHA$ is 153.2° .

Figure 4.7 shows how each cavity in **16**_{CH₂Cl₂} is also bounded by four metallocycles, but in this case the pocket contains only one (disordered) molecule of dichloromethane. If the guest-accessible void is viewed as passing through metallocycles 2 and 3 (as numbered in Figure 4.7), then the space is terminated by the iodides of metallocycles 1 and 4 (shown as pink spheres). The single guest molecule still effectively templates the assembly of the molecular “hexagons”. In **16**_{CH₂Cl₂} the host iodide and guest chlorine atoms are within van der Waals contact of one another, $I \cdots Cl = 3.514(12) \text{ \AA}$ while the sum of van der Waals radii = 3.78 \AA (see footnote[‡] about the radius of iodide). The volume of the solvent-filled cavity of **16**_{CH₂Cl₂} is 132.5 \AA^3 and that of **16**_{CHCl₃} is 158.6 \AA^3 . These volumes are significantly larger than those in the structures already mentioned, almost certainly as a result of the size of the chlorinated guest molecules.

The metallocycle derived from $CdBr_2$ (**17**_{MeOH}) is similar to that shown in Figure 4.6 and a figure is therefore not provided. The bromide van der Waals radius is slightly larger ($r = 1.93 \text{ \AA}$; 1.80 \AA for Cl) and the cavity size is calculated to be 127 \AA^3 ($r_{\text{probe}} = 1.4 \text{ \AA}$). In the case of **17**_{MeOH}, the methanol guest forms a hydrogen bond with the bromide with $D \cdots A = 3.326(5) \text{ \AA}$.

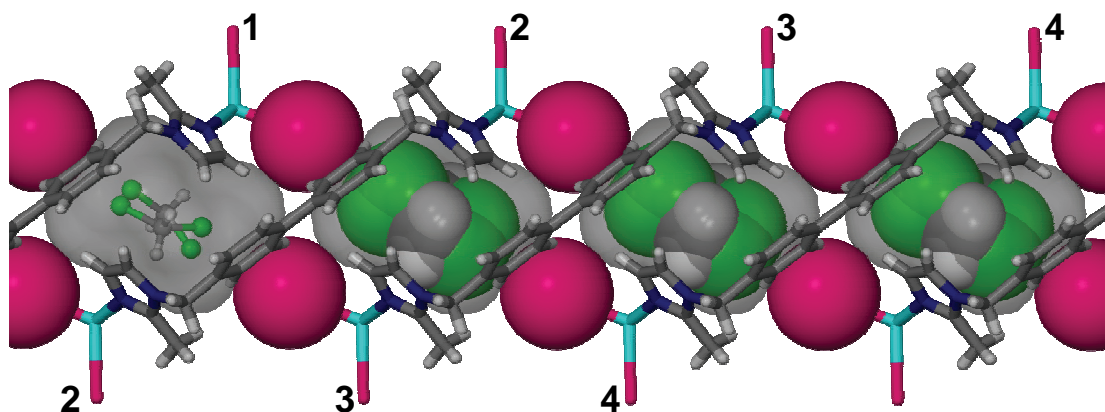


Figure 4.7 Columnar stacking of **16**_{CH₂Cl₂} along [001] (horizontal direction) viewed down the *b*-axis. The neutral complexes are shown as capped-sticks and the guest molecules are shown in ball-and-stick in the left-most cavity and van der Waals representation in the remaining cavities. Connolly surfaces (using a probe radius of 1.4 \AA) of the solvent-filled pockets are shown in semi-transparent grey. Host metallocycles of $[Cd_2L_2I_4]$ are shown with one disordered dichloromethane guest molecule per cavity. Disorder is shown over only two positions for clarity, but the final model involves disorder over eight positions. The guest-accessible voids have volumes of *ca* 133 \AA^3 in the case of **16**_{CH₂Cl₂} and 159 \AA^3 in the case of **16**_{CHCl₃} (not shown).

[‡] If the supposed value of the van der Waals radius of I⁻ is used (2.20 \AA), the sum of the radii of Cl and I⁻ = 4 \AA .

The metalloclusters (**13-17**) stack along [001] to form columns, each of which is in contact with four neighbouring columns as shown in Figure 4.8.

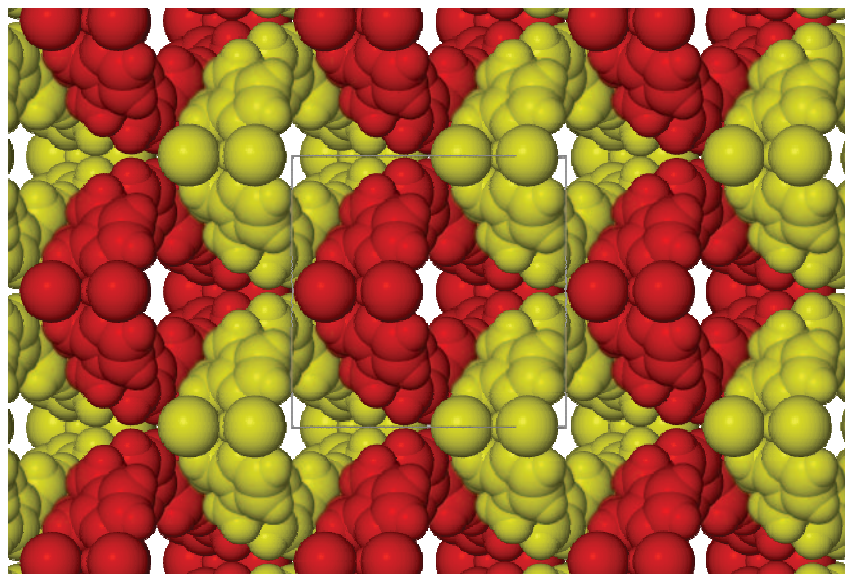


Figure 4.8 Space-filling projection showing packing of the stacked metalloclusters that are illustrated in Figure 4.6 and Figure 4.7. The two colours distinguish adjacent columns of host molecules that are not related by simple translation, viewed along [001]. The guest molecules have been omitted for clarity.

Although **17**_{MeOH} forms a metallocluster as described above, careful observation of the crystals revealed concomitant formation of another crystal form which was also

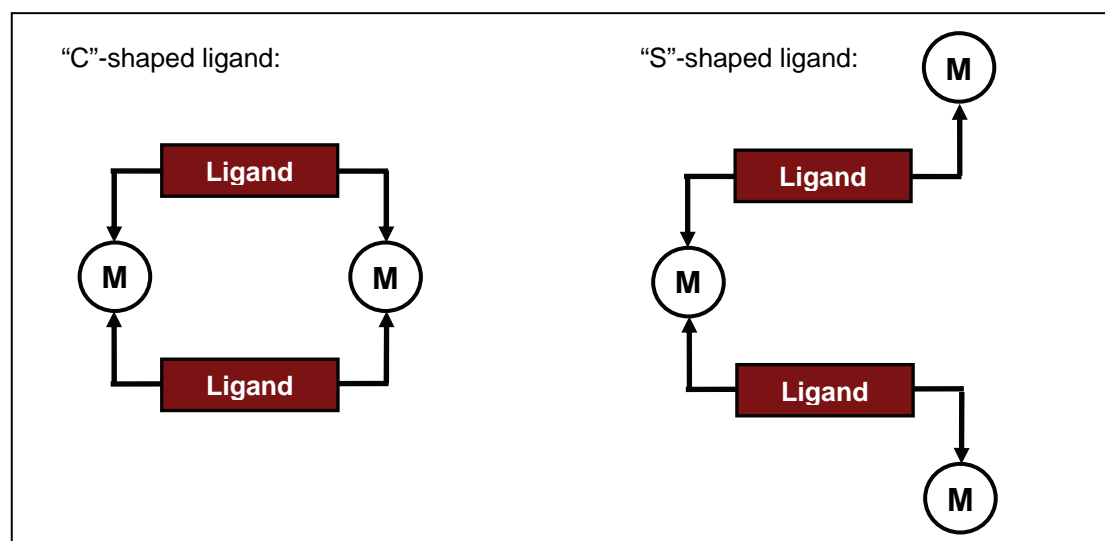


Figure 4.9 Schematic showing "C"-shaped *converging* structures and "S"-shaped *diverging* structures.